RESEARCH ARTICLE | OCTOBER 17 2023

Helicity and dissipation correlation in anisotropic turbulent flow fields Θ

Oanh L. Pham (0); Dimitrios V. Papavassiliou (20)



Physics of Fluids 35, 105135 (2023) https://doi.org/10.1063/5.0160336





CrossMark

Articles You May Be Interested In

Novel features of a fully developed mixing-layer between co-flowing laminar and turbulent Couette flows

Physics of Fluids (March 2014)

Photoelectron imaging using an ellipsoidal display analyzer

Rev Sci Instrum (June 2001)

Shear-layer dynamics at the interface of parallel Couette flows

Physics of Fluids (October 2022)





20 October 2023 02:34:59

Helicity and dissipation correlation in anisotropic turbulent flow fields

Cite as: Phys. Fluids **35**, 105135 (2023); doi: 10.1063/5.0160336 Submitted: 31 May 2023 · Accepted: 24 September 2023 · Published Online: 17 October 2023



ARTICLE





Oanh L. Pham 🕞 and Dimitrios V. Papavassiliou 🗈 🕞

AFFILIATIONS

School of Sustainable Chemical, Biological and Materials Engineering The University of Oklahoma 100 East Boyd, SEC T-335 Norman, Oklahoma 73019, USA

^{a)}Author to whom correspondence should be addressed: dvpapava@ou.edu. Tel.: (405) 325-5811

ABSTRACT

The relation between the helicity and the rate of dissipation of turbulent kinetic energy in turbulent flows has been a matter of debate. Herein, direct numerical simulations of turbulent Poiseuille and Couette flow were used in combination with the tracking of helicity, helicity density, and dissipation along the trajectories of passive scalar markers to probe the correlation between helicity and dissipation in anisotropic turbulence. The Schmidt number of the scalar markers varied between 0.7, 6, and infinite (i.e., fluid particles), while the friction Reynolds number for both simulations was 300. The probing tools were the autocorrelation coefficients, the cross correlation coefficients between helicity and dissipation, and the joint probability density function calculated in the Lagrangian framework along the positions of the scalar markers. These markers were released at different locations within the flow field, including the viscous wall sublayer, the transition layer, the logarithmic region, and the outer flow. In addition, conditional statistics for scalar markers that dispersed most or least in the flow field were also calculated. It was found that helicity and dissipation changed along the trajectories of scalar markers; however, helicity and dissipation were not correlated in the Lagrangian framework. There was anticorrelation between helicity and dissipation in the near wall region, which was less obvious in the logarithmic region. More importantly, helicity could be used to characterize the alignment of the fluctuating velocity and vorticity vectors along the trajectories of scalar markers that disperse the farthest in the direction normal to the channel wall.

Published under an exclusive license by AIP Publishing. https://doi.org/10.1063/5.0160336

I. INTRODUCTION

Helicity is a topological variable that can be viewed as a measure of the degree of the knottedness or the linkage of the vortex lines in a flow field and the degree of broken symmetry. 1-3 Helicity appears in flow fields associated with natural phenomena, such as hurricanes, tornadoes, and rotating "supercell" thunderstorms in the atmosphere, and in Langmuir circulations in the oceans. Moreover, it plays an important role in the evolution of turbulent flows, as it is one of only two inviscid invariants (kinetic energy and helicity) in three dimensional (3D) turbulence. The total helicity in a flow, \mathcal{H} , is defined as a volume integral in the flow field $\mathcal{H} = \int \mathbf{u} \cdot \boldsymbol{\omega} dV$, where \mathbf{u} is the velocity vector and ω is the vorticity vector. The inner product of velocity and vorticity is called the helicity density, H, $(H = u \cdot \omega)$. Helicity, helicity density, and kinetic energy play important roles in understanding the nonlinear dynamics, intermittency, and topology of fluid turbulence.

The topological relevance of helicity is explained mainly by the works of Moffatt, Speziale, and Biferale.^{2,9–12} However, these papers do not consider anisotropic turbulence and hence they do not apply directly to internal flows and wall turbulence, which is the objective of the present study. The literature review below includes this work, the findings on homogeneous and isotropic turbulence, and the literature with rotating flows. Out of this prior work, it emerges that the connection of helicity and the rate of dissipation of the turbulent kinetic energy (TKE) is still under debate.

In general, it has been found that asymmetries and anisotropy are needed to generate helicity in turbulence. In addition to its topological character, one may consider the dynamic perspective to helicity so that it becomes important in anisotropic turbulent flows (including swirl flows and rotating turbulence) and then to anisotropic turbulence close to wall. The dynamical systems perspective starts from the physics literature and generalized Hamiltonian dynamics, where it has been demonstrated that helicity enters as a constitutive variable to inviscid flows within the framework of the so-called Nambu-Blender-Névir mechanics. Since helicity is topologically and dynamically conserved, this constrains the scale-to-scale transfer processes. In some instances,

backscattering effects have been reported, which are neglected in turbulence closure models used in Reynolds-averaged Navier–Stokes and large eddy simulations (LES). Backscatter, however, can be important as seen in the demixing of rotational flows by excitation and emission of helical shear waves. ^{13–15}

According to Blender, Nambu mechanics can be extended to incompressible ideal hydrodynamical fields using kinetic energy and helicity in 3D, where both helicity and energy are quantities that are conserved as integrals. If the flow is homogeneous, it has been shown that helicity cannot contribute to the generation and sustainment of large scale structures. 16 There is a need to have some type of asymmetry in the flow for the generation of vorticity and by extension rotational flow structures, 17 as has been confirmed with magnetorhydrodynamic studies. 18 Since the Reynolds stress tensor in turbulence is symmetric, it follows that helicity itself cannot contribute to the Reynolds stress and thus to the production of turbulent kinetic energy. It has also been pointed out that the presence of turbulent helicity density alone is insufficient, and other factors breaking the symmetry, such as compressibility, anisotropy, mean flow, are necessary for the generation of large-scale vortical flow. 19 However, in the Lagrangian sense, along the trajectories of scalar particles dispersing in turbulent flow, the Reynolds stress tensor is not symmetric.20

A recent *Science* article²¹ showed for the first time that experimental measurements of helicity are possible, opening up opportunities to revisit the role of helicity in turbulence with new investigative tools. "Helicity is of key importance in turbulent thermal convection, it is vital to understand how helicity inhibits the energy cascade to small scales at which turbulent energy is dissipated as heat," as stated in the *Perspectives* section of the same issue of *Science*. Since vorticity and velocity are difficult to measure experimentally, only a few studies on helicity in anisotropic and inhomogeneous turbulent flow are available. Simulations for rotating flows have been utilized. For comparisons between rotating and non-rotating flows, direct numerical simulation (DNS) results showed that in rotating flow, helicity has a major impact on the decay rate of the kinetic energy.²²

One can distinguish two types of helicity studies, namely, studies on the emergence of helicity and studies on the effects of helicity on the dynamics of turbulence. Since helicity is a conserved quantity for inviscid incompressible 3D flow, it is often examined in terms of a cascade, similar to the turbulent kinetic energy (TKE) cascade from large scale flow structures to small scale structures. In this way, helicity and the rate of TKE dissipation, ϵ , have been connected in the literature through theory and computations. Note that the TKE is known to cascade from large scales to small scales in turbulence, until it is dissipated into heat when the scales are small enough for viscous dissipation to be effective.

Many studies have concentrated on homogeneous turbulence.²³ Choi *et al.* carried out a DNS of forced isotropic turbulence to find that there is little correlation between helicity and dissipation.²⁷ Biferale *et al.* simulated fully developed homogeneous and isotropic turbulence to investigate the transfer properties of energy and helicity fluctuations.¹² In other work, the cascade of TKE and helicity, as well as the development of two-equation models for Large Eddy Simulations (LES) that can include helicity were investigated.^{28,29} For rotating inhomogeneous turbulence, it was shown that the pressure diffusion term of the Navier–Stokes equations can involve the turbulent helicity gradient so that inhomogeneous helicity is important in

the generation of the large-scale velocities in incompressible turbulent flows. ²³ Recently, helicity density and normalized helicity density were investigated for various cases of flow in lid-driven cavity. ²⁵ Yu *et al.* investigated the spatial distributions, multiscale distributions, and inter-scale transfer of helicity in turbulent channel flows with streamwise rotation to provide theoretical suggestions for LES modeling in these cases where the flow is different than homogeneous and isotropic turbulence. ³

By and large, the role of helicity in turbulence and its influence on TKE redistribution remains a matter of debate. ^{18,23,28–31} According to Moffatt, high relative helicity density should be correlated with low energy dissipation rate and vice versa. ^{32,33} Other studies have explored whether helicity density could be an indicator of the dissipation levels in a flow field. Orlandi *et al.* considered a rotating pipe in which the flow symmetry was disrupted by the rotation and a mean helicity was present. They showed that when helicity increased, the dissipation was reduced. ³⁴

Even in flows that are not rotating, the Navier–Stokes equations for momentum can be written as

$$\frac{\partial \mathbf{u}}{\partial t} + \boldsymbol{\omega} \times \mathbf{u} = -\nabla \left(p + \frac{1}{2} |\mathbf{u}|^2 \right) + \nu \nabla^2 \mathbf{u},\tag{1}$$

utilizing the vector identity $(\boldsymbol{u}\cdot\nabla)\boldsymbol{u}=\boldsymbol{\omega}\times\boldsymbol{u}+\frac{1}{2}\nabla(\boldsymbol{u}\cdot\boldsymbol{u})$. In the above equation, p is the pressure, t is the time, and ν is the dynamic viscosity of the fluid. Now, it becomes apparent that the non-linear term of the Navier–Stokes equation can be replaced by the Lamb vector $\boldsymbol{\omega}\times\boldsymbol{u}$. Since the turbulent kinetic energy is produced through this non-linear term, the Lamb vector can be considered to be the term that leads to the TKE cascade. On the other hand, the following equation holds:

$$|\mathbf{u} \cdot \mathbf{\omega}|^2 + |\mathbf{u} \times \mathbf{\omega}|^2 = |\mathbf{u}|^2 |\mathbf{\omega}|^2. \tag{2}$$

This equation can be verified by considering $\frac{|u\cdot\omega|^2}{|u|^2|\omega|^2}+\frac{|u\times\omega|^2}{|u|^2|\omega|^2}=1$, since $\cos^2\theta+\sin^2\theta=1$, where θ is the angle between the velocity and vorticity vectors. Therefore, TKE cascade to smaller scales is less intense when the term $u\times\omega$ is small and $u\cdot\omega$ is large, so that regions that are helical are expected to have relatively low dissipation. Therefore, it has been argued that the cascade is prevented in flow regions with high helicity density $\mathbf{u}\cdot\mathbf{\omega}$. $\mathbf{v}\cdot\mathbf{v}$. In other words, when the velocity and vorticity vectors are aligned, the nonlinear energy transfer is inhibited.

Other theoretical analysis suggested that low dissipation could be associated with either low or high helicity when the Lamb vector was decomposed into irrotational and solenoidal parts. Rogers and Moin used DNS of homogeneous turbulent flow and channel flow to report that there is no correlation between relative helicity density and the rate of dissipation of TKE in homogeneous turbulent flows. For channel flow, the study showed that except for low dissipation regions near the outer edge of the buffer layer, there was no tendency for flow to be helical. Thus, the simulations did not indicate that relative helicity is associated with low dissipation or with coherent structures.

However, a relationship between dissipation and helicity may be revealed when one calculates a conditional probability density function (PDF) for the relative helicity density. The condition can be on high or low values of $S_{ij}S_{ij}$, where S_{ij} is the local rate of strain tensor for the local fluctuating velocity. Using Einstein's summation convention, the rate of dissipation of TKE, ϵ , is $\epsilon = 2\nu \overline{S_{ij}S_{ij}}$, where $S_{ij} = \frac{1}{2}(\frac{\partial u_i'}{\partial x_i} + \frac{\partial u_j'}{\partial x_i})$,

and u_i' is the fluctuating velocity in the i direction. Conditioning on large or small values of $S_{ij}S_{ij}$, allows to examine the relative helicity density in regions of high or low ϵ . Experiments for a turbulent boundary layer, turbulent two-stream mixing layer, and a turbulent grid flow have been conducted to examine the properties of the relative helicity density. The probability of the total velocity and vorticity vectors to be aligned was found to increase with distance from the wall. In general, there has been little documentation of a relationship between small instantaneous dissipation rate and large relative helicity density except in the regions of the high shear rate, where all instantaneous dissipation rate amplitudes were small compared to the largest values occurring in the whole flow domain. Altogether, it appears that the interaction mechanism between energy and helicity dynamics is complex and it is often unclear, even more so in anisotropic turbulent flows $\frac{1-3+12}{1-3+12}$

On the other hand, other studies focused on the role of helicity in turbulent transport using a Lagrangian framework. Nguyen and Papavassiliou applied DNS of turbulent channel flow with friction Reynolds number $Re_{\tau}=300$ in conjunction with Lagrangian tracking of fluid particles and passive scalar markers for Schmidt number, Sc, equal to 0.7 and 200 to calculate local helicity along trajectories of mass markers and fluid particles. The Lagrangian helicity distribution indicated that a change of the alignment between velocity and vorticity vectors occurs for scalar transport markers, and the scalar transport was enhanced as this alignment was more prominent. 5

The present work aims to elucidate the role of particle-path properties that are associated with scalar transport in wall turbulence. The correlation between the rate of TKE dissipation and helicity can be important in this investigation, since one could hypothesize that low dissipation regions of the flow potentially could be identified by helicity. In the sections that follows, we probe this correlation as we probe the question of whether scalar transport is enhanced in regions of high or low velocity and vorticity alignment (i.e., high or low helicity density)

A Lagrangian approach provides a natural way to investigate turbulent dispersion, in turbulent heat/mass transport.20 Therefore, the combination of DNS and Lagrangian scalar tracking (LST) could be beneficial in studying turbulent transport. Lagrangian techniques were used because they are very well-suited for simulating scalar transport in both low, but mainly high, Sc regimes from 6 to 2400.³⁵ In anisotropic turbulence, the interplay between convection and diffusion is critical.^{36,37} These methods have also been utilized to study the principal direction of transport of heat (or mass) for both forward on time and backward in time single particle dispersion.²⁰ Several other groups have taken further advantage of Lagrangian algorithms for a deeper understanding of turbulent mixing and transport, for example, to study the relative dispersion of fluid particle pairs to wall-bounded turbulent flows,³⁸ and to study dispersion and deposition of particles in Poiseuille and Couette flows.³⁹ Our research group also combined DNS and LST to study chemical reactions in turbulent flow, 40, transfer, 42,43 dispersion, and mixing 36,44,45 and to predict the turbulent Prandtl number in wall turbulence.4

In this study, the DNS is combined with LST to simulate Poiseuille and Couette flows and compute the velocity of particles at different Schmidt number, *Sc.* The calculations provided the total helicity and the helicity of the fluctuating velocity field, as well as the rate of dissipation of the TKE in the Lagrangian framework. Statistical

analysis was used to evaluate the correlation between helicity and dissipation. In this way, one can make inferences about the use of helicity as an indicator to characterize the level of energy cascade. Two canonical configurations of wall-bounded flow are the Poiseuille and Couette flow. 47 Poiseuille flow is the pure pressure-driven fluid motion in channels with fixed walls, while Couette flow is the pure shear-driven motion of a fluid between walls that are moving relative to each other. 48,49 Because of the difficulties of achieving fully developed flow in a long channel with a moving wall, experiments for Couette flow are limited.⁵⁰ In turbulent Couette flow, it has been found that the outer flow in the region close to the channel center contains large-scale lowand high-speed regions extending over a very long streamwise distance. 51,52 The reason is that a fully developed plane Couette flow has a constant shear stress across the entire channel, making the outer region look like a very extended logarithmic region (see the supplementary material section for turbulent flow statistics). Furthermore, the value of the gradient of the mean velocity is not zero at the Couette flow center, meaning that there is production of TKE at the channel center, contrary to Poiseuille flow, where the mean velocity gradient is zero in the channel center, leading to zero production of TKE. This characteristic allows for a significantly different character to the flow in this region, when compared to pressure-driven channel flow. 53-55 The main issue for computations of Couette flow is the existence of long and wide structures, which have been found to exist both experimentally and numerically. This means that there is a need for long computational boxes to capture these structures, making the study of this flow more computationally expensive than turbulent Poiseuille flow.

This study includes the following sections. Section II: description of the numerical methods and the parameters used for the direct numerical simulation and the Lagrangian scalar tracking, as well as the numeric procedures for the post processing of the data; Sec. III: results and discussion for the helicity density in the Eulerian frame, details of the correlation between helicity and dissipation in a Lagrangian framework and the effects of helicity on scalar transport for different Sc scalars, and the correlation of helicity and flow structure with its effects on turbulent transport; and Sec. IV: conclusions about the role of helicity and its connection to the dissipation of TKE in turbulent transport.

II. NUMERICAL METHODS

A. Flow field generation

In this study, the pseudospectral DNS algorithm presented by Lyons et al. 57,58 and validated by the experiments of Gunther et al. 5 was applied to simulate turbulent channel flow. This algorithm has been modified and used to simulate plane Couette flow. 37,49,60,61 The DNS employed three fractional steps to describe the time evolution of the velocity field. The first fractional step considered the non-linear convective terms of the Navier-Stokes equations, with a semi-implicit, second-order accurate Adams-Bashforth-Crank-Nicholson scheme. The inviscid contribution of the dynamic pressure head was computed in a second fractional step using an implicit Euler scheme. The viscous effects were taken into account in the third fractional step. The computations were conducted using dimensionless variables. The friction velocity, $u^* = (\tau_w/\rho)^{1/2}$, where τ_w is the wall shear stress and ρ is the fluid density, and the fluid kinematic viscosity, ν , were used to define the friction length scale, $l^* = \nu/u^*$, and the friction timescale, $t^* = l^*/u^*$, so that all quantities were scaled in viscous wall units.⁵⁷ From this point on, in this manuscript all quantities presented in the text and

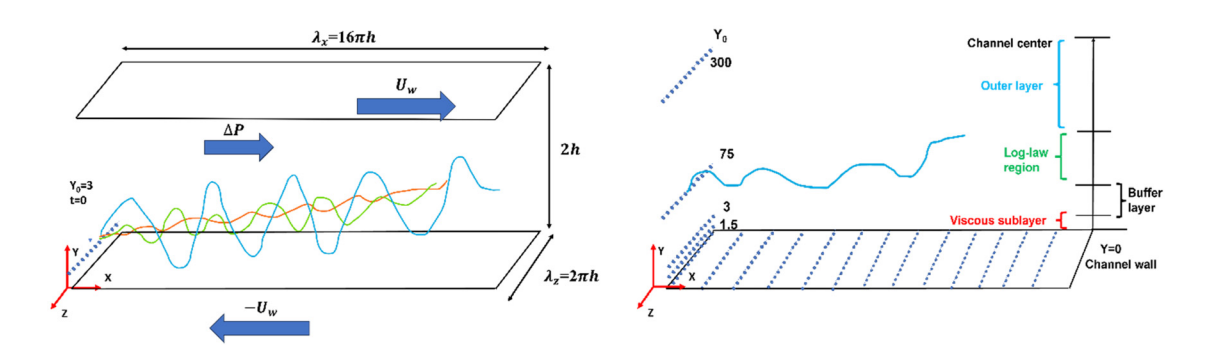


FIG. 1. Left panel: Sketch of the simulation setup with an indication of the box size and exemplary particle trajectories. The blue line represents a particle path for moderately small Schmidt number (Sc = 0.7) with strong diffusion, the green line a particle path for moderately large Schmidt number (Sc = 0.7) with weak diffusion, and the red line the path of a fluid particle ($Sc \to \infty$). The prescribed forcing is sketched for Poiseuille flow ($dP/dx \neq 0$, $U_w = 0$) and Couette flow (dP/dx = 0, $U_w \neq 0$). Right panel: Sketch of a particle path with respect to the boundary layer structure for the conventional normalization of the wall-normal coordinate. Selected marker release wall distances are given by dotted lines.

figures are normalized with the wall parameters, unless specified otherwise. The dimensions of computational box were $16\,\pi h \times 2h \times 2\pi h$ for both Poiseuille and Couette flow in the streamwise x, normal y, and spanwise z directions, respectively. The half channel height was h=300 in viscous wall units, so that the friction Reynolds number was also $Re_\tau=h=300$. The number of grid points was $1024\times 128\times 256$ for Poiseuille and $1024\times 256\times 256$ for Couette flow in the x, y, and z directions. As for Couette flow, the walls of the channel moved relative

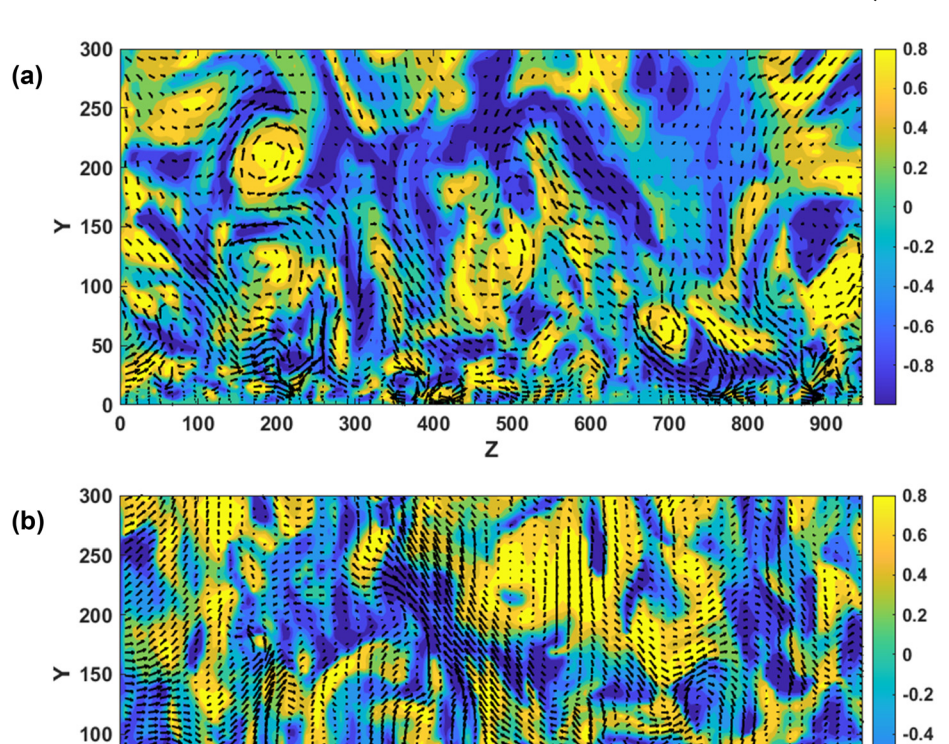
to each other, while there was no mean pressure gradient. Therefore, in Couette flow the code was modified by changing the Dirichlet boundary conditions, so that the streamwise velocity at the wall $U_{\rm w}$ was

$$U_w = \pm Gh, \tag{3}$$

and G was constant (G = 0.064). The top wall of the channel moved in the negative x direction and the bottom wall moved in the positive x direction. The Reynolds number defined for Poiseuille flow based on

-0.6

-0.8



500

Z

600

700

800

400

FIG. 2. Vector plot for the velocity field superimposed on the contour plot of relative helicity density at the spanwise-wall normal plane (yz plane), at x=3786 and at time t=100 for (a) Poiseuille flow and (b) Couette flow. Half of the channel is shown, with the center of the channel located at Y = 300 and the bottom wall at Y = 0

200

300

50

the mean centerline velocity and the half channel height, $Re = (U_c h/\nu)$ and for Couette flow as $Re = (U_w h/\nu)$, was 5700. The fluid was assumed to be an incompressible Newtonian fluid with constant properties. At the channel walls, the no-slip, no-penetration boundary condition was utilized, while periodic boundary conditions were applied in the streamwise and spanwise directions. The transport equations in these two directions were expanded by Fourier series, and the vertical velocity and pressure head were expanded in terms of a Chebyshev polynomial series, which provided adequate resolution to satisfy rigid boundary condition. The time step for the simulation of Poiseuille flow was $\Delta t = 0.1$, and for Couette flow it was $\Delta t = 0.05$.

B. Lagrangian scalar tracking (LST)

In a Lagrangian framework, the system of reference moves with fluid particles. In Lagrangian scalar tracking (LST), the trajectories of individual scalar markers were monitored as described in a thesis by Kontomaris. Scalar markers were released into the flow after the channel and Couette flow reached stationary state. Simulations were conducted for different cases of Sc: Sc = 0.7, 6 and the case of fluid particles. The Schmidt number is defined as $Sc = \nu/D$, D is the molecular diffusivity. Note that in this manuscript, the terminology used is related to mass transfer and the Sc, even though all results are applicable for

heat transfer characterized by the Prandtl number, Pr, (defined as $Pr = \nu/\alpha$, α is the molecular thermal diffusivity) of the dispersing scalar markers when there is no production or consumption of mass. The Pr = 0.7 and 6 correspond to the case of air and water, which are the most typical fluids in practical applications. The case of fluid particles is associated with the very large Pr or Sc number. These values span several orders of magnitude and are sufficient—we have seen in prior work that data for very high Sc can be grouped together, 37,42,67 data for low Sc can be grouped together and the Sc = 6 case is in the transition region of Sc.

Assuming that the Lagrangian velocity at time t of a marker released at location X_o is the same as the Eulerian velocity of the fluid at that particle's location at the beginning of the convective step $V(X_o,t)=U[X(X_o,t),t]$ (U is the Eulerian velocity vector of the fluid at the location of the marker at time t), one can integrate in time to obtain the convective part of the scalar marker motion. A mixed sixth-order Lagrangian–Chebyshev interpolation scheme was used to calculate the velocity vector between grid points. The markers moved because of convection in the flow field, and because of molecular diffusion. According to Einstein's theory for Brownian motion, the diffusion effect was computed by adding a 3D random walk on the particle motion at the end of every convection step. A Gaussian distribution with zero mean and a standard deviation of $\sigma = \sqrt{2\Delta t/Sc}$ in viscous wall units could be utilized to create the size of the random jump in each one of

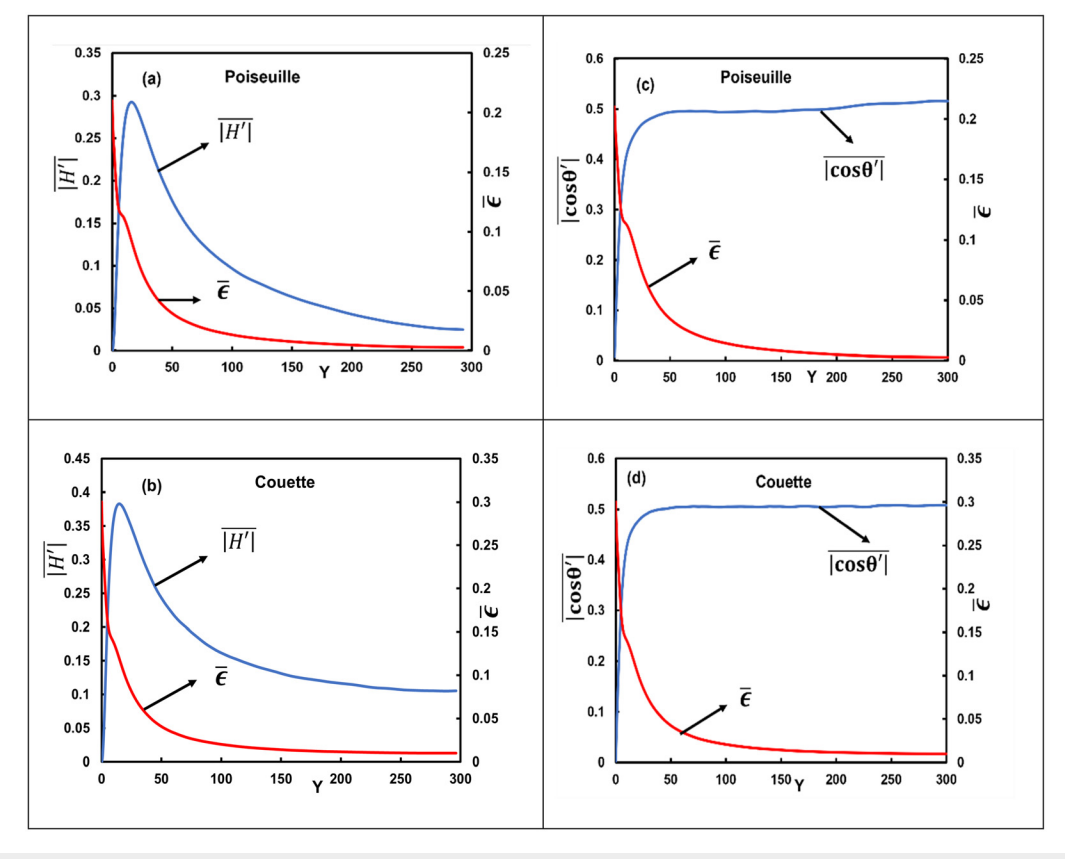


FIG. 3. The Eulerian mean of the absolute values of fluctuating helicity density $(|H'| = |u'.\omega'|)$ for (a) Poiseuille flow and (b) for Couette flow. Mean absolute value of the relative helicity density $(|h'| = |\cos\theta'|)$ calculated as a function of distance from the wall for (c) Poiseuille flow and (d) Couette flow. The red line is the mean of the rate of TKE dissipation $(\bar{\epsilon})$ in the Eulerian framework corresponding to the Poiseuille and Couette flow.

the three space directions. The equation of particle motion was integrated using an Adams–Bashforth scheme. The advantage of the LST methodology is that it is applicable to an extensive range of Sc.⁶⁷

Scalar markers were released at given distances Y_0 (in viscous length units) from the bottom wall of the computational channel, $Y_0=0,\,1.5,\,3,\,5,\,10,\,15,\,75,$ and 300 for both Poiseuille and Couette flow. These release positions represent the channel wall, the viscous wall sublayer, the buffer region, the logarithmic layer, and the

channel center. The particle release at $Y_0=1.5$ is within the viscous wall sublayer (where $y=\overline{U}$), the release at $Y_0=5$ is at the edge of the viscous sublayer, $Y_0=10$ and 15 are in the transition layer, and the release at $Y_0=75$ is in the log layer where the distance from the wall is proportional to the logarithm of the mean velocity of the flow. The logarithmic layer extends to about a quarter of the channel half height for Poiseuille flow, and all the way to the channel center for Couette flow. In Fig. 1, we present a schematic of the

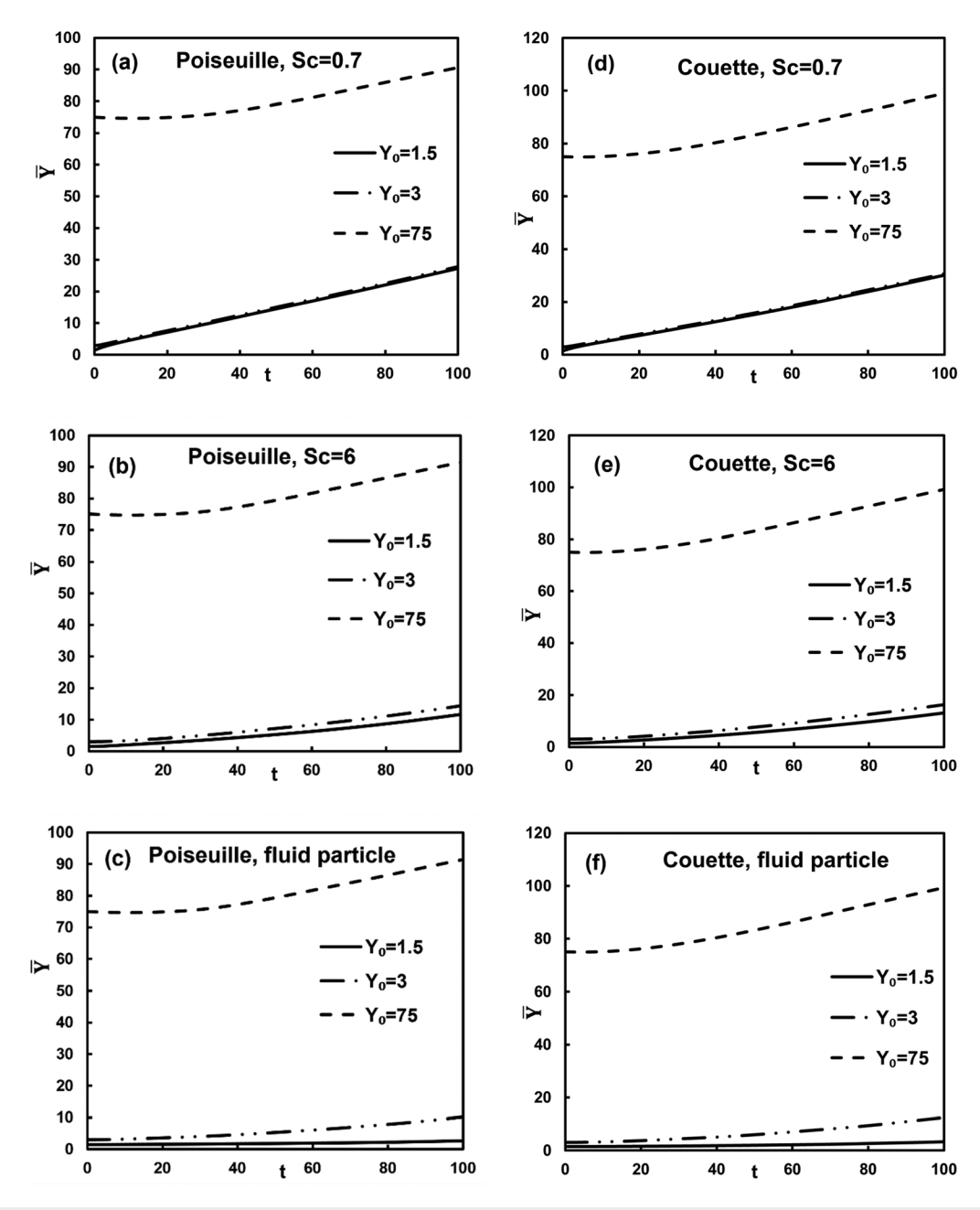


FIG. 4. The average position of particles at release positions $Y_0 = 1.5$, 3, 5, and 75 in Couette flow and Poiseuille flow at various Sc numbers. Poiseuille flow (a) Sc = 0.7, (b) Sc = 6, (c) fluid particle; Couette flow (d) Sc = 0.7, (e) Sc = 6, and (f) fluid particle.

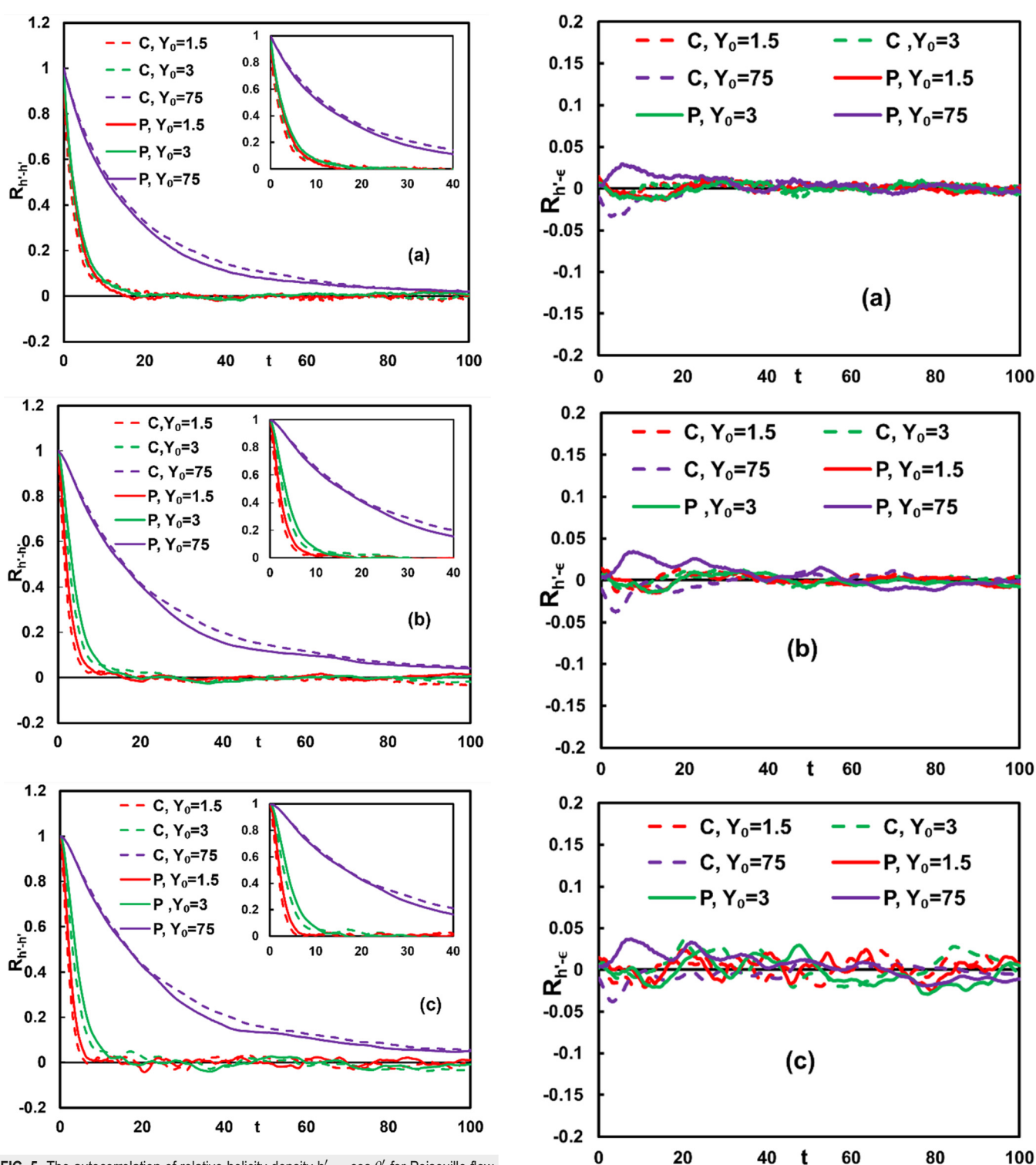


FIG. 5. The autocorrelation of relative helicity density $\mathbf{h}' = \cos\theta'$ for Poiseuille flow and Couette flow at (a) Sc = 0.7, (b) Sc = 6, and (c) fluid particles. The symbol P on the legend represents results for Poiseuille flow and the symbol C represents Couette flow. The insets highlight the differences between different areas of release at early simulation times.

FIG. 6. The Pearson cross correlation between the relative helicity density $h'=\cos\theta'$ and the dissipation for Poiseuille flow and Couette flow at (a) Sc=0.7, (b) Sc=6, and (c) fluid particles.

computational setup and the locations of the particle release locations in relation to the regions of the flow. At each Y_0 , 100 000 particles were released from 20 lines that were uniformly spaced in the x direction while spanning the width of the channel in the z direction. This was done to avoid bias that could be potentially caused by the turbulent velocity field at the instant of marker release. Therefore, the total number of particles released in the flow field was 800 000 for either Couette or Poiseuille flow.

C. Post-processing

Using LST, data for position, velocity, vorticity, and for the derivative of the velocity in each of the three directions were obtained along the trajectory of each particle in the flow. To calculate the fluctuating velocity and the derivatives of the fluctuating velocity at each time step, the mean velocity \overline{U} and the derivative of the mean velocity $d\overline{U}/dy$ in the Eulerian framework were used to obtain the mean velocity and its derivative at each particle position in the y direction. A weighted average of the two values connected by a straight line was used. ⁶⁸

The fluctuating velocity vector, u', and its derivatives in the three space directions were used to calculate the vorticity vector for the fluctuating velocity, ω' . The relative normalized helicity density is defined as $h' = \cos \theta'$, where θ' is the angle between the fluctuating velocity and vorticity vectors⁶⁹

$$\mathbf{h}' = \cos \theta' = \frac{\mathbf{u}' \cdot \mathbf{\omega}'}{(|\mathbf{u}'||\mathbf{\omega}'|)},\tag{4}$$

where $u' = u - \overline{U}$, and $\omega' = \nabla \times u'$. When the velocity and vorticity vectors align with each other, then h' = 1 and when they are perpendicular to each other, h' = 0.

The turbulent dissipation rate along the trajectories of each marker was calculated as 26

$$\epsilon = 2\left(\frac{\partial u'}{\partial x}\right)^2 + 2\left(\frac{\partial v'}{\partial y}\right)^2 + 2\left(\frac{\partial w'}{\partial z}\right)^2 + \left(\frac{\partial u'}{\partial y} + \frac{\partial v'}{\partial x}\right)^2 + \left(\frac{\partial u'}{\partial z} + \frac{\partial w'}{\partial x}\right)^2 + \left(\frac{\partial v'}{\partial z} + \frac{\partial w'}{\partial y}\right)^2.$$
 (5)

The statistical analysis was based on calculations of correlation coefficients and joint pdfs. The joint PDF $P(\epsilon, h')$ can demonstrate how h' is distributed for all values of ϵ and is a useful tool to define what conditions on ϵ yield regions that are helical in nature. In this case, a 2D array of bins were generated that represented different values of ϵ and h'. The number of scalar markers that had values within the range of each bin was counted and then the probability was calculated by dividing by the total number of particles.

The autocorrelation for relative helicity density and dissipation was evaluated as follows:⁷⁰

$$R_{h'-h'(t)} = \frac{\overline{h'(t_0)h'(t_0+t)}}{\overline{h'(t_0)^2}},$$
 (6)

$$R_{\epsilon-\epsilon(t)} = \frac{\overline{\epsilon(t_0)\epsilon(t_0+t)}}{\overline{\epsilon(t_0)^2}},$$
 (7)

where t_0 is the time at which the particles are released into the flow field. The cross correlation between relative helicity density and

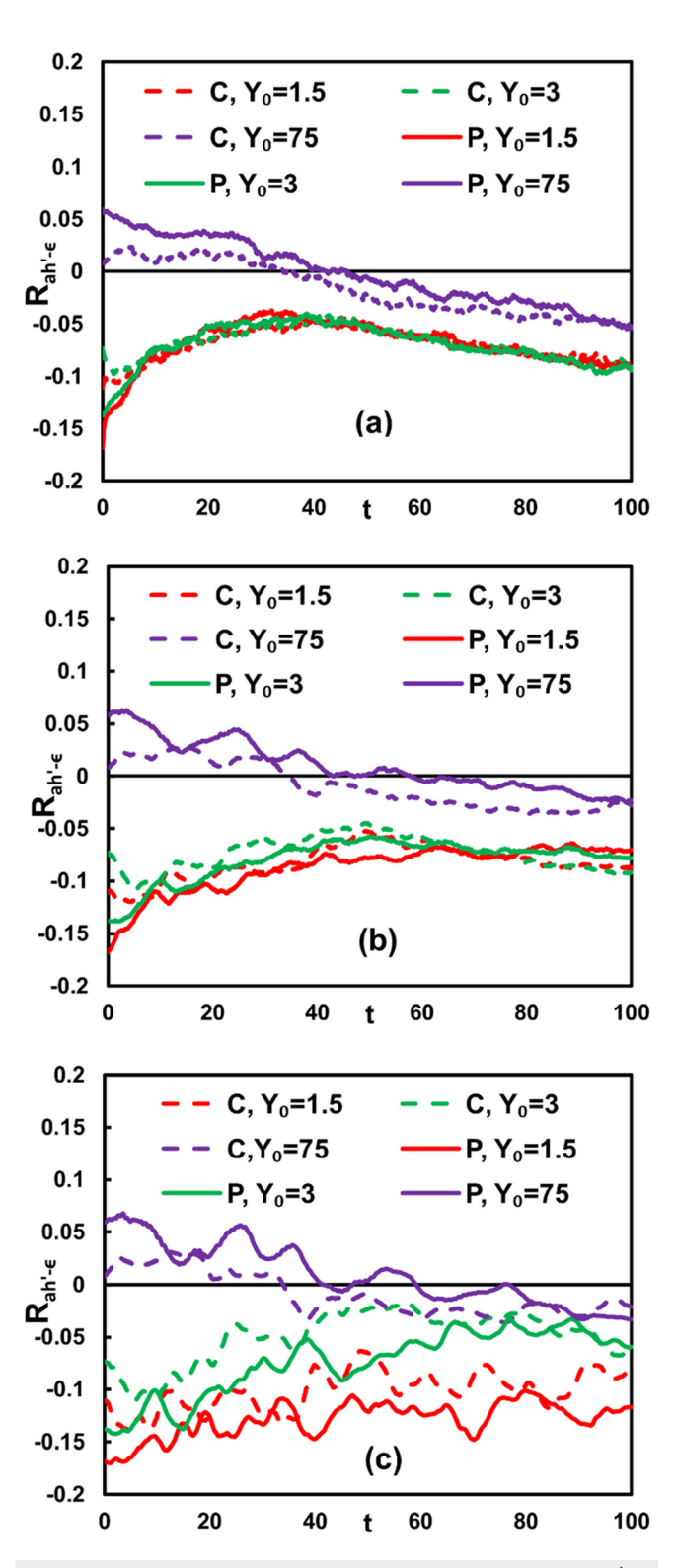


FIG. 7. The Pearson cross correlation between ϵ and absolute value of h' for Poiseuille flow and Couette flow at different *Sc*: (a) Sc = 0.7, (b) Sc = 6, and (c) fluid particles.

dissipation was calculated by the Pearson cross correlation formula as follows:

$$R_{\mathbf{h}'-\epsilon} = \frac{\sum_{i=1}^{n} \left(\mathbf{h}'_{i} - \overline{\mathbf{h}'}\right) \left(\epsilon_{i} - \overline{\epsilon}\right)}{\sqrt{\sum_{i=1}^{n} \left(\mathbf{h}'_{i} - \mathbf{h}'\right)^{2}} \sqrt{\sum_{i=1}^{n} \left(\epsilon_{i} - \overline{\epsilon}\right)^{2}}}.$$
 (8)

The overbars above represent the ensemble average over n scalar particles, while the index i designates individual particles and its range is from 1 to the total number of particles, which is $100\,000$ for each case of particle release. It is $n=100\,000$ when all particles per one release position are considered, and it is $n=25\,000$ when considering only the quartile of particles that move the farthest or the closest to the wall.

III. RESULTS AND DISCUSSION

The vector plots for the velocity field superimposed on the contour plot of relative helicity density at the yz plain are shown in Fig. 2, and the profiles of the mean of the absolute value of the helicity of the fluctuating velocity field, |H'|, and the absolute value of the relative helicity density for Poiseuille and Couette flow are presented in Fig. 3. The values shown were obtained in the Eulerian sense, as averages over time and space. Positive or negative helicity can have similar effects in turbulent transport, so the absolute value is used instead of the actual value, to make sure that the positive and negative helicity values do not average to zero. For Poiseuille flow, the mean of the absolute helicity increases from 0 at the wall to a maximum at a position within the buffer layer, at about 20 viscous wall units away from

the wall. The absolute helicity then declines gradually to reach a local minimum at the center of the channel. The absolute values of the relative helicity density (h' = $\cos\theta'$) increase from the channel wall to about 0.5 at Y = 50, and then appear to be almost constant with distance from the wall. The velocity and vorticity vectors tend to be at about 60° from each other beyond Y = 50, while they were perpendicular to each other at very low Y. Meanwhile, when it comes to Couette flow, the profile of |H'| and |h'| exhibit a trend like Poiseuille flow but |H'| has higher values than for Poiseuille flow. The alignment of velocity and vorticity on average (as seen when considering h') is the same in Poiseuille and in Couette flow.

The average positions of particles released at $Y_0 = 1.5$, 3, and 75 of Couette flow and Poiseuille flow at various Sc number are presented in Fig. 4. The markers moved farther from the wall and the average position of particles increased faster for Sc = 0.7 than for Sc = 6 and for fluid particles. This can be explained by the fact that the particles with smaller Sc are influenced more by Brownian motion. The random motion of the tracked particles follows a PDF with standard deviation that increases when Sc decreases, as seen in Sec. II. These scalar markers can escape the viscous wall region at earlier simulation times and then diffuse with larger displacement because of larger molecular diffusion (smaller Sc). The root mean square particle displacement in the normal direction for Poiseuille and Couette flows and various Sc numbers are shown in Fig. S1 in the supplementary material.

The effect of Sc on the autocorrelation coefficient of the relative helicity density of the fluctuating velocity can be seen in Fig. 5. As mentioned already, computations have been carried out for different locations of particle release ($Y_0 = 0$, 1.5, 3, 5, 10, 15, 75, and 300).

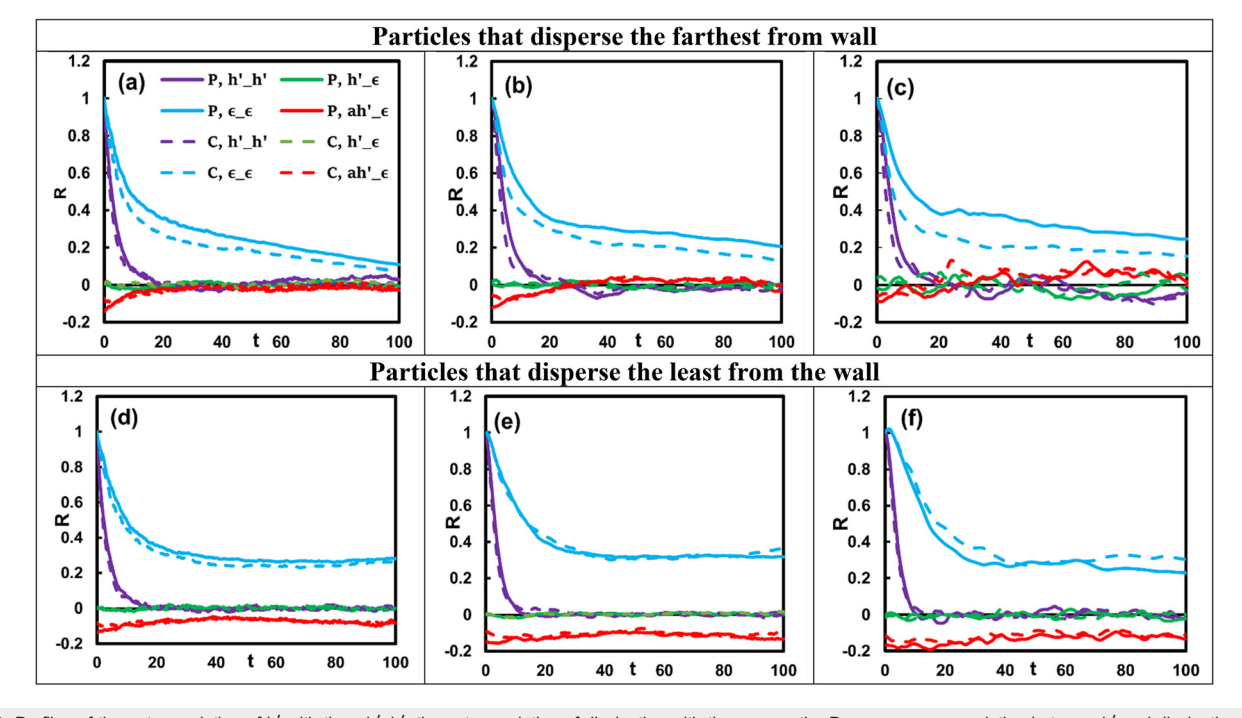


FIG. 8. Profiles of the autocorrelation of h' with time, h'_h'; the autocorrelation of dissipation with time, $\epsilon = \epsilon$; the Pearson cross correlation between h' and dissipation h' $= \epsilon$; and the Pearson cross correlation of the absolute value of = 0.7, with dissipation, ah' = 0.7. The correlations for the 25% of the particles that were found to be the farthest from the wall at t = 100 are shown in the top row: (a) = 0.7, (b) = 0.7, (c) fluid particles. The correlations for the 25% of the particles that were found to be the closest to the wall at t = 100 are shown in the bottom row: (d) = 0.7, (e) = 0.7, (f) fluid particles. The particles that were released at = 0.7, (e) = 0.7, (e) = 0.7, (f) fluid particles. The particles that were released at = 0.7, (e) = 0.7, (e) = 0.7, (e) = 0.7, (f) fluid particles. The particles that were released at = 0.7, (f) = 0.7, (g) = 0.7, (e) = 0.7, (f) = 0.7, (g) = 0.7, (g) = 0.7, (e) = 0.7, (f) = 0.7, (f) = 0.7, (f) = 0.7, (g) = 0.7, (e) = 0.7, (f) = 0.7, (f) = 0.7, (f) = 0.7, (f) = 0.7, (g) = 0.7, (g) = 0.7, (e) = 0.7, (f) = 0.7, (f) = 0.7, (f) = 0.7, (g) = 0.7, (g) = 0.7, (e) = 0.7, (f) = 0.7, (f) = 0.7, (f) = 0.7, (g) = 0.7, (g) = 0.7, (e) = 0.7, (f) = 0.7, (f) = 0.7, (g) = 0.7, (g) = 0.7, (e) = 0.7, (f) = 0.7, (f) = 0.7, (g) = 0.7, (g) = 0.7, (e) = 0.7, (

Among these, we present cases that have physical meaning (e.g., release inside the viscous sublayer at $Y_0 = 1.5$ and 3, and in the logarithmic layer at $Y_0 = 75$). The supplementary material section includes results for more cases. The data presented highlight differences between positions of release. The coefficient decreased most significantly during the first 20 viscous time units for $Y_0 = 1.5$ and 3 for both Couette and Poiseuille flows. As can be seen, the autocorrelation decreases slower when the position of marker release (Y_0) is farther from the wall. These values decreased to about zero after 30 dimensionless time units. However, when the particles were released in the logarithmic layer at $Y_0 = 75$, the autocorrelation coefficient remained larger than zero for the duration of the simulations. This trend is

significant for the case of fluid particles [see Fig. 5(c)] and following that is the case of Sc = 6. For Sc = 0.7, there seems to be minimal change in the autocorrelation profile at $Y_0 = 1.5$ and 3 for both Couette and Poiseuille flows. In general, it appears that the autocorrelation of the relative helicity density depends on the particle release position and on the Sc rather than whether the flow is Poiseuille or Couette. Based on the law of the wall and based on turbulent flow similarity at the inner region for wall turbulence, it is reasonable to assume very little difference between the near wall turbulence structure for Couette flow and Poiseuille flow. However, DNS work has showed that the peak of maximum streamwise intensity of Couette flow is higher than that for Poiseuille flow and the logarithmic region in

ARTICLE

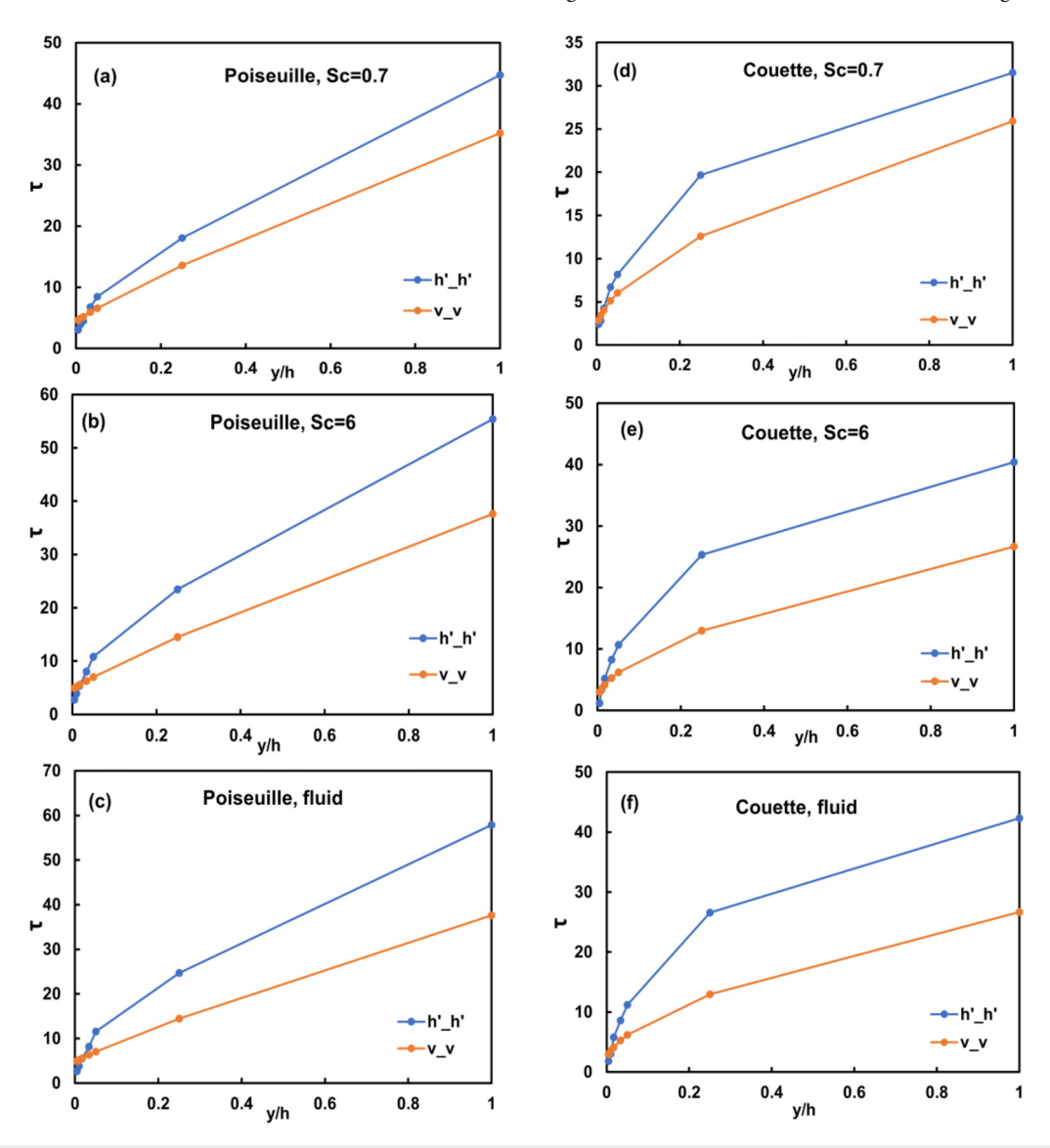


FIG. 9. The Lagrangian timescale as a function of source elevation for dispersion in the *y*-direction for different Sc numbers and types of flow where the vertical axis is timescale and the horizontal axis is $\frac{Y_0}{\hbar}$ (Y_0 is the initial position of release particles) for the relative helicity density $h' = \cos\theta'$ (h'_-h') and velocity from prior results (v_-v_+) from Ref. 37) for Poiseuille flow at (a) Sc = 0.7, (b) Sc = 6, and (c) fluid particles and for Couette flow at (d) Sc = 0.7, (e) Sc = 6, and (f) fluid particles. The lines are used to guide the eye between data points.

Couette flows is much wider than the one that can be found in turbulent Poiseuille flow at similar Reynolds numbers. ^{49,56} The outer region structure, therefore, is different in the two cases. The channel flow has lower levels of turbulent velocity fluctuations than the Couette flow at the centerline and the Couette flow has stronger turbulent velocity fluctuations throughout the domain. ⁷² Therefore, one can see that the profile of the correlation in our study is similar for Couette and Poiseuille flow, but the Couette flow shows a steeper decrease in the correlation that could be explained by the wider logarithmic layer region in Couette flow that makes particles move off the buffer layer

faster and demonstrated a decrease in the correlation. The timescale for helicity seems to be short, less than 20 viscous time units.

To examine the correlation of h' with the rate of dissipation of the turbulent kinetic energy ϵ , the cross correlation coefficient was determined along the trajectories of the passive markers in the flow and presented in Fig. 6. It is apparent that the correlation values fluctuate within a small range around the value of zero and do not show any trend with time in any of the cases studied. This leads to the suggestion that there was no correlation between ϵ and h'. Regions of low (or high) helicity do not correspond to regions of high (or low) dissipation,

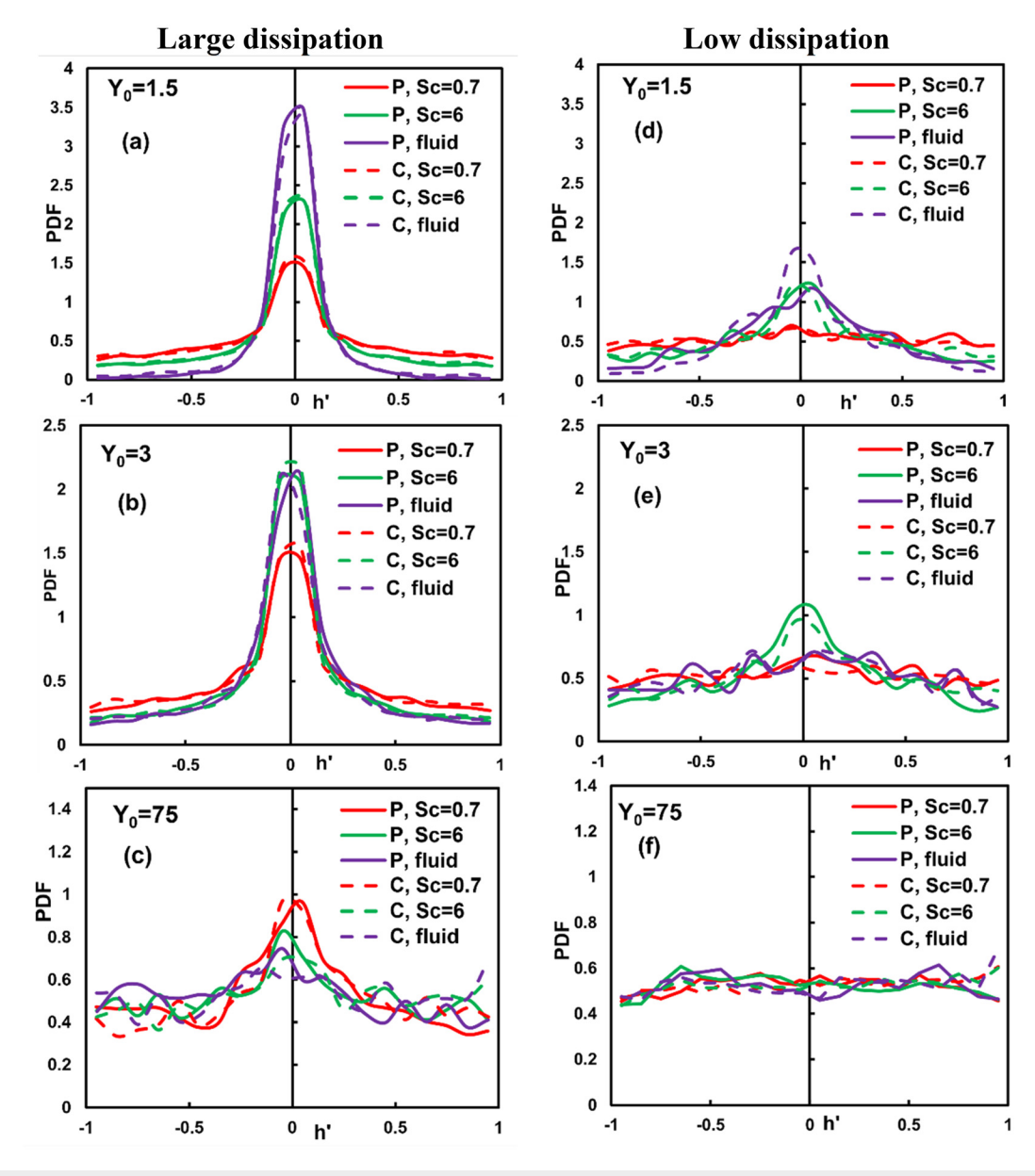


FIG. 10. The distribution of relative helicity density $h' = \cos \theta'$ conditional on high rate of TKE dissipation (left column) at (a) $Y_0 = 1.5$, (b) $Y_0 = 3$, (c) $Y_0 = 75$ and low dissipation (right column) at (d) $Y_0 = 1.5$, (e) $Y_0 = 3$, and (f) $Y_0 = 75$ at t = 100 for Poiseuille (P) and Couette flow (C). For Couette and Poiseuille flow, the high dissipation is more than 8 times and 10 times the average dissipation, respectively, and the low dissipation is less than 0.25 times the average dissipation.

indicating that the energy cascade to very small scales is not related to the relative alignment of the velocity and vorticity vectors along the trajectories of scalar particles in the flow.

When calculating the cross correlation between the TKE dissipation rate and the relative helicity density, the cosine can be positive or negative, while ϵ is positive. Therefore, the correlation values fluctuate within a small range around the value of zero. However, when one considers the absolute value of the relative helicity, it is found that the relative helicity density and the dissipation are anticorrelated. The Pearson cross correlation between ϵ and the absolute value of h' is represented in Fig. 7. In this case, the sign of the angle between the vorticity and velocity vector is not important. The results are interesting: consider the case of fluid particles where the lowest values of the cross correlation coefficient appear for fluid particles released within the viscous wall sublayer, at the position $Y_0 = 1.5$ and for both types of flow. For release farther from the wall, the correlation gets to higher values but is still negative, except for Y₀= 75, where cross correlation values are positive right after particle release, but then fall to less than 0. This case is similar to the case for Sc = 6. When Sc = 0.7, the values of $R_{\mathbf{h}' - \epsilon}$ were negative but not significantly different between $Y_0 = 1.5$, 3, and 5. From these figures, one may conclude that the relative helicity density and the dissipation are anticorrelated. This anticorrelation is not complete since the values of the cross correlation do not go as low as -1. There are many particles that have dissipation larger than the average values, the corresponding h' is smaller than average, but this does not occur with all particles.

Whether helicity can be used to identify flow structures that are major contributors to turbulent dispersion has been explored in the past. The hypothesis was that regions with high values of helicity, if they also exhibited low dissipation, they could indicate flow structures that would tend to persist in time, making them candidates for strong contributors to turbulent transport.⁵ In order to examine this relationship between helicity and turbulent transport further, we now focus on the particles that were transported the farthest from the wall in the normal direction, y. We chose to examine the scalar markers that were released at $Y_0 = 3$ as a typical case for transport away from the viscous wall subregion. The particles that failed to disperse were also examined, to differentiate between high dispersion and low dispersion. The results are seen in Fig. 8. We chose the top quartile, i.e., the 25% of the particles that moved the farthest away from the wall at the end of the simulation and compared their behavior to the bottom quartile, i.e., the 25% of the particles that remained closer to the wall at the end of the simulation. The quartiles are quite often used in statistics as a selected part of a sample to represent the right side (high random

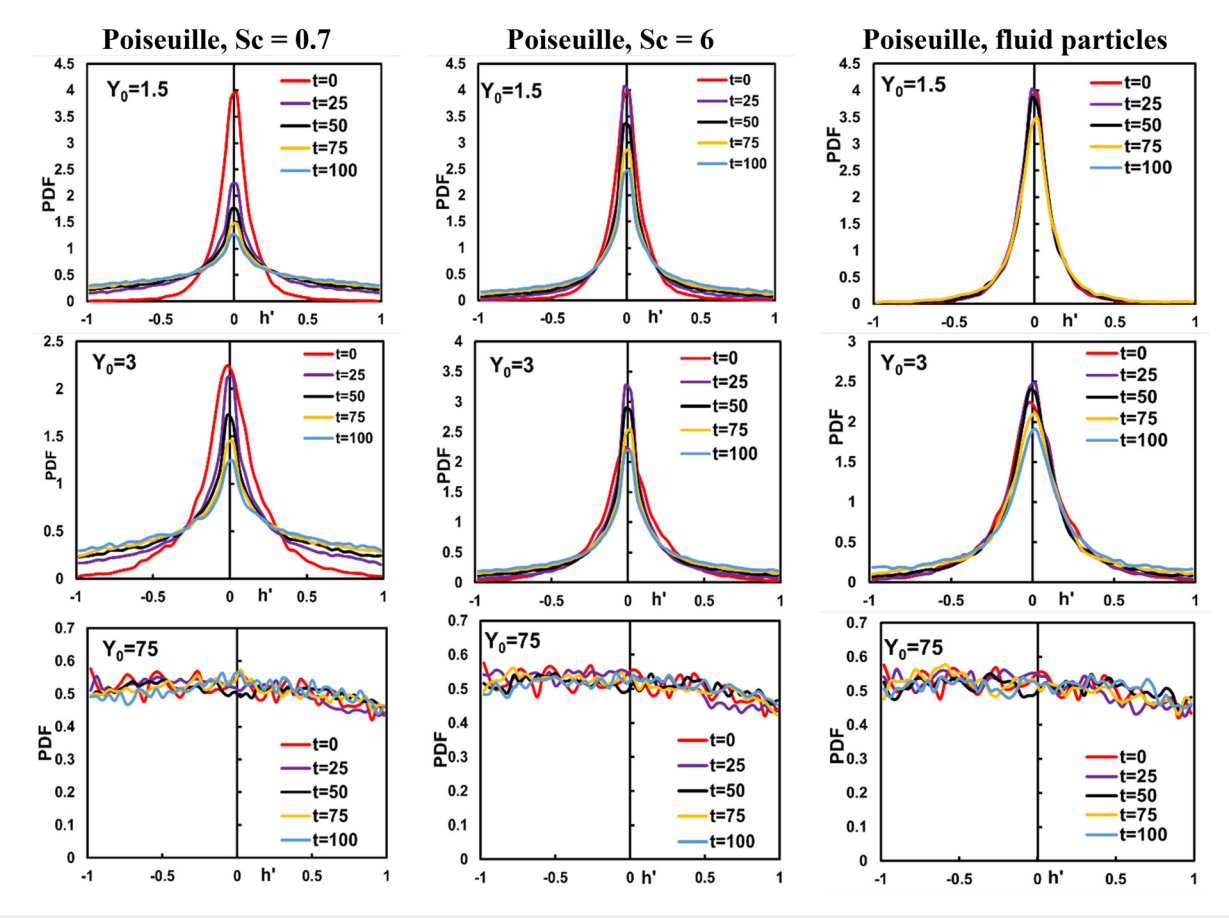


FIG. 11. The distribution of relative helicity density $h' = \cos\theta'$ at various times for a release position at $Y_0 = 1.5$, 3, and 75 of Poiseuille flow with Sc = 0.7, 6, and fluid particles. Columns correspond to Sc, and rows to positions of release.

variable values) and the left side (low random variable values) of a PDF. In our case, the top and bottom quartiles include 25 000 particles, and we consider this to be a large enough sample size to obtain statistical information. We could have used 20% or 30%, and we would be getting similar results. However, the quartiles are typical in statistical reporting. The autocorrelation for h' and ϵ for particles that dispersed farthest and closest to the wall was also evaluated. This coefficient remained positive, but it declined slowly with time for the top quartile of dispersing particles. It tended to stay constant for long times for the particles that were closer to the wall (see the bottom row of Fig. 8). Therefore, particles that stayed in flow structures of similar h', and did not go through flow regions where the alignment of velocity and vorticity changed, remained closer to the wall.

The Pearson cross correlation between h' and ϵ is very small for the cases of Sc=0.7 and 6, but this value fluctuated more for fluid particles. There were no differences between the top and bottom quartiles of particles. When it comes to the autocorrelation of ϵ , this value decreased within the first 20 time units and then gradually declined with time for all cases, but with different slope for various Sc and for the farthest and closest particles. The autocorrelations and the Pearson cross correlations for Poiseuille and Couette flow at Sc=0.7 and 6 also display the same trends for the

particles closer to the wall, while the particles that disperse the farthest from the wall in Poiseuille flow showed a decrease in helicity correlation that is slower than that for Couette flow. The dissipation correlation shows a faster decline for Couette flow in comparison to Poiseuille flow.

However, there is a difference in the Pearson cross correlation of the absolute value of the relative helicity density h' and ϵ for the farthest and closest particles. The particles close to the wall have constant values around -0.2 for both types of flows and different Sc number, while for the farthest particles, the value of the cross correlation started at about -0.2 and then approached zero for all cases. This leads to the suggestion that there is an effect of helicity on the transport of scalars from the wall, in the sense that helicity density is an indicator of lower than average dispersion.

The autocorrelation coefficients can be used to define characteristic timescales for the dispersion of the scalar. Dispersion is the mean squared of the particle displacement relative to their source, as defined by Taylor, who introduced the statistical description of turbulent dispersion from a Lagrangian perspective. The dispersion Lagrangian timescale can be obtained as a function of the elevation from the wall of the scalar source, Y_0 , in the *y*-direction, and can be calculated as 37

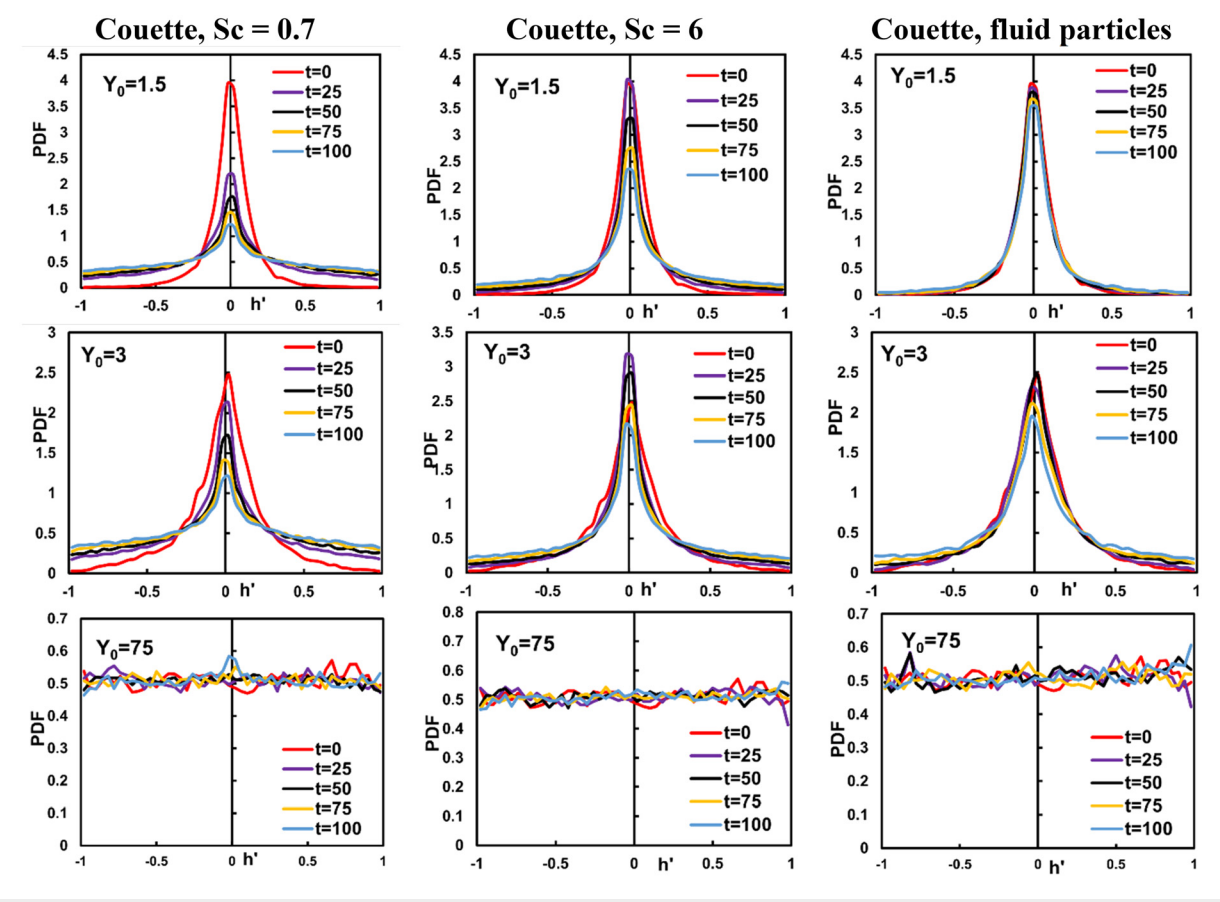


FIG. 12. The distribution of relative helicity density $h' = \cos \theta'$ at various times for release position $Y_0 = 1.5$, 3, and 75 for Couette flow with Sc = 0.7, 6, and fluid particles. Columns correspond to Sc and rows to positions of release.

$$\tau_{Ly} = \int_{t_o}^{\infty} R_{h'-h'}(t, t_o) dt. \tag{9}$$

As can be seen from Fig. 9, the newly defined timescale was a function of the position of scalar release, and it increased to its highest value for scalar release at the center of the channel. For Couette flow, the largest timescale had values between 30 and 45 viscous time units, meanwhile that of Poiseuille flow was higher, in the range of 45-55. A similarly defined Lagrangian timescale for the vertical fluctuating velocity has been reported in a prior study from our laboratory³⁷ and its values are plotted in Fig. 9 for comparison. It was found then, as it is found now, that the timescale for Poiseuille flow is more sensitive to the Sc and is higher than for Couette flow. However, the timescale for helicity is much larger than the timescale for velocity, indicating that the flow structure has stronger effects on turbulent transport than what one would expect based on fluid velocity considerations. The dispersing particle velocity may decorrelate from the conditions at the time of release in the flow, but transport may still depend on the flow structure at the point of particle release.

The probability density functions (PDFs) for h' have been calculated and displayed in Fig. 10. A distinction between the particles that

were found in areas of low and high ϵ was made. For Couette and Poiseuille flow, the high ϵ was defined to be more than 8 times and 10 times the average ϵ , respectively, and the low dissipation was defined to be less than 0.25 times the average dissipation. The main criterion was to have enough particles in the high and low ϵ cases to be able to obtain meaningful statistics from the analysis. The values 10 (for Poiseuille), 8 (for Couette), and 0.25 (for the low ϵ for both Poiseuille and Couette) were determined as follows: First, the mean rate of TKE dissipation $\overline{\epsilon}$ was calculated in the Eulerian framework for Poiseuille and Couette flow. Then the particles that had high or low ϵ were defined as those whose values of ϵ were larger or smaller than c or m times of $\overline{\epsilon}$ ($\epsilon > c\overline{\epsilon}$ for the high case, and $\epsilon < m\overline{\epsilon}$ for the low dissipation case). After examining options for the values of c and m, the coefficients chosen were those that did not lead to a very large or a very low number of particles for all 8 positions of particle release, if 2%-25% of the total number of particles were represented, then this was good enough for analysis.

The PDF for particles that have the highest ϵ show a peak around the value of zero. This indicates that the velocity and the vorticity vectors for particles in areas of high dissipation of TKE tend to be perpendicular to each other. Far from the wall the PDFs appear to be flatter, so the probability of having velocity and vorticity vectors that align in

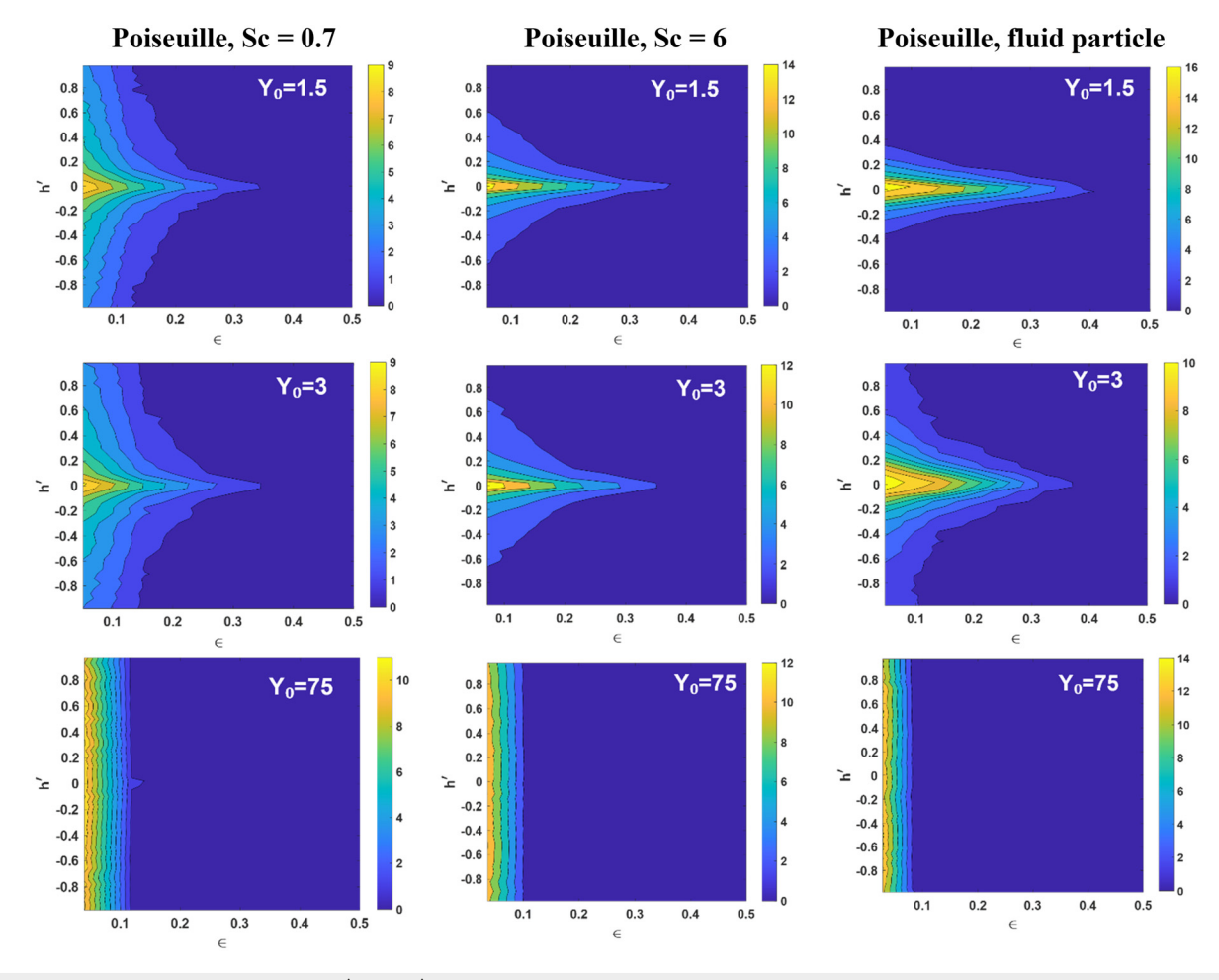


FIG. 13. Joint PDF of relative helicity density $h' = \cos \theta'$ and the rate of TKE dissipation (ϵ) for all particle of Poiseuille flow for different Sc numbers at time t = 100.

areas of high dissipation is smaller than closer to the wall. However, when considering the Sc, it is seen that the lower the Sc the flatter the PDFs are (meaning that the tails of the PDFs are higher and the peaks are lower as Sc decreases). On the other hand, the PDF for the helicity h' of particles that are in locations of low ϵ are much flatter in comparison. This shows that for regions with low dissipation, the distribution of h' is more uniform. The vorticity and velocity vectors do not have an alignment that favors a 90° angle—which was the case for high dissipation. The alignment seems to be more random. Furthermore, there does not appear to be a Sc effect on flatness of the PDF. On the other hand, for the particles with high dissipation, their h' distribution has been affected by Sc and the position of release rather than the flow configuration.

Figures 11 and 12 show the distribution of h' at various times for different release positions and Sc for Poiseuille and Couette flow, respectively. For both Couette and Poiseuille flows, at $Y_0 = 1.5$, 3, at t = 0 the PDF is narrow around zero, and then it widens as time advances. The meaning of this finding is that the vorticity and velocity vectors are mostly perpendicular when the particles are release, but as the particles disperse away from the wall, the vorticity and velocity

vectors start to align (note the elevated values of the PDFs at +1 and -1 in Figs. 9 and 10 as time advances). Moreover, the Sc=0.7 case showed the most dramatic decrease in the intensity of the PDF peaks with time, the Sc=6 exhibited the same trend but with less pronounced peaks. The profiles of the PDF for fluid particles did not change much with time. This can be explained by considering the Brownian motion of particles at low Sc. These particles have large Brownian motion and could disperse faster to regions farther from the wall (see Fig. 4). For $Y_0=75$, the distribution of helicity is flat and does not change with time or Sc. Therefore, it can be concluded that farther from the wall, the values of normalized fluctuating helicity were larger and the velocity and vorticity vectors were more aligned to each other rather than being perpendicular to each other.

The joint PDF between the relative helicity density and the dissipation for Poiseuille flow and Couette flow at Sc = 0.7, 6 and fluid particles is shown in Figs. 13 and 14, respectively. At the release position $Y_0 = 1.5$, the case for fluid particles has the narrowest range of distribution of h' from -0.4 to 0.4 for Poiseuille flow and -0.3 to 0.3 for Couette flow, while Sc = 6 has the wider range from -0.6 to 0.6 for Poiseuille flow and -1 to 1 for Couette flow. For Sc = 0.7, the values

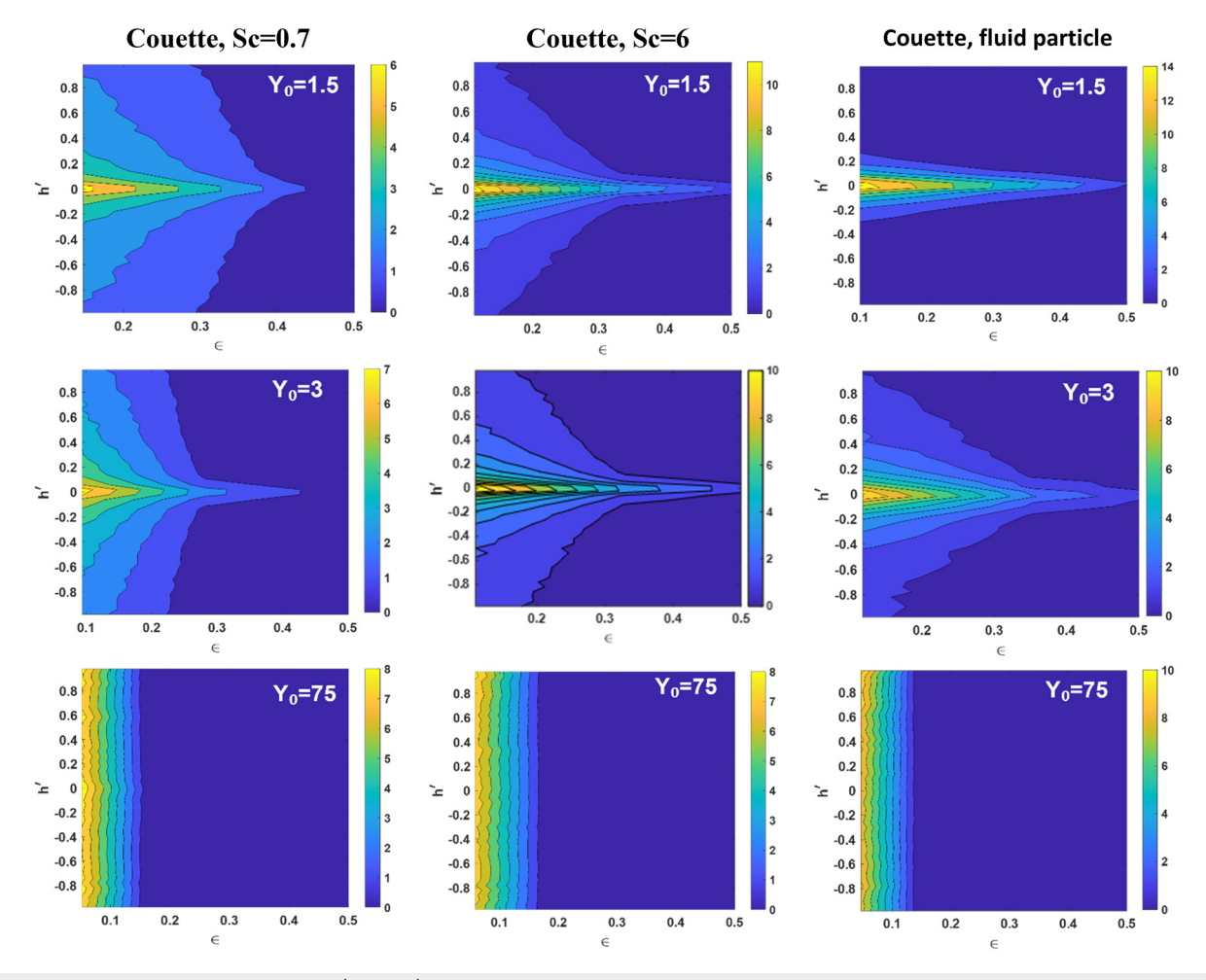


FIG. 14. Joint PDF of relative helicity density $h' = \cos \theta'$ and the rate of TKE dissipation (ϵ) for all particles of Couette flow for different Sc numbers at time t = 100.

are in the range of -1 to 1 for both types of flow. Farther from the wall, the distribution of h' is wider, from -1 to 1. The physical interpretation of these results is that the probability of particles that are in locations where the fluctuating velocity and vorticity vectors are perpendicular is high from $Y_0 = 1.5$ to $Y_0 = 5$ (the plot for $Y_0 = 5$ and $Y_0 = 300$ are provided in supplementary material section). However, the cosine of the angle between vorticity and velocity is evenly distributed from -1 to 1 for a scalar release position within the log layer region. More importantly, from these patterns, it is seen that low h' does not necessarily associate with high dissipation and vice versa. These results agree with Rogers and Moin that there is no obvious relation between helicity of the fluctuating velocity field and the dissipation of TKE.

IV. SUMMARY AND CONCLUSIONS

In this study, the relative helicity and the rate of dissipation of TKE along passive particle trajectories were tracked in a Poiseuille channel and a plane Couette flow using direct numerical simulation and Lagrangian scalar tracking. The changes of helicity and dissipation were monitored along the trajectories of scalar markers as a function of time. The autocorrelation of fluctuating relative helicity density and the Pearson cross correlation between helicity and dissipation were computed. The joint PDF between relative helicity density and dissipation was also presented.

It was found that there is no positive correlation between helicity and dissipation, and flow regions with low dissipation do not necessarily indicate regions of high helicity. This result is in agreement with the previous study of Rogers and Moin⁶ and the theory of Speziale. In fact, an anticorrelation between helicity density and dissipation is observed, which is more pronounced in the viscous sublayer and becomes very weak in the logarithmic layer. In regions of low dissipation, the distribution of the helicity density is more uniform than in regions of high dissipation, indicating a more random alignment between fluctuating velocity and vorticity vectors. On the other hand, both the position of release of the particles and the *Sc* number have noticeable effects on the helicity experienced by a passive particle. The type of flow, whether it is Couette or Poiseuille, does not appear to play a significant role.

Regarding turbulent transport, there appears to be an effect of helicity, but not because of an association of helical flow structures to low TKE dissipation. The Lagrangian timescale for helicity density is longer than the Lagrangian timescale for velocity, showing that the alignment of the vorticity and velocity vectors relative to each other is important for long time duration. The particles that disperse less over the simulation period are those that exhibit a strong anticorrelation between the helicity density and dissipation, while the helicity autocorrelation coefficient is positive and larger than for particles that disperse the most. In this respect, helicity can be an indicator of low turbulent dispersion. The PDFs of the helicity density indicate that as particles transport away from the channel walls, they tend to be in flow regions where the vorticity and velocity vectors tend to align with each other, rather than staying perpendicular to each other. It is apparent that the relationship between helicity and turbulent scalar transport needs further evaluation in the future. Specifically, there is a need to probe the helicity along particle trajectories that are transported the farthest from the wall and its correlation with flow structure characteristics other than dissipation, such as the Reynolds stress using quadrant analysis, and the orientation of the eigenvectors of the rate of strain tensor.

SUPPLEMENTARY MATERIAL

The supplementary material included data for the standard deviation of the particle location distribution in the direction vertical to the channel walls, data on the turbulent velocity statistics, and data of the joint PDF for helicity density and the rate of TKE dissipation that complement Figs. 13 and 14.

ACKNOWLEDGMENTS

Financial support of the National Science Foundation (Grant No. CBET-1803014) was gratefully acknowledged, as is the use of computing facilities at the University of Oklahoma Supercomputing Center for Education and Research and at XSEDE (under allocation CTS-090025).

AUTHOR DECLARATIONS

Conflict of Interest

The authors have no conflicts to disclose.

Author Contributions

Oanh L. Pham: Conceptualization (equal); Data curation (lead); Formal analysis (lead); Investigation (equal); Methodology (equal); Validation (lead); Visualization (lead); Writing – original draft (equal); Writing – review & editing (equal). Dimitrios V. Papavassiliou: Conceptualization (lead); Formal analysis (equal); Funding acquisition (lead); Investigation (equal); Methodology (equal); Project administration (equal); Resources (lead); Supervision (lead); Writing – original draft (equal); Writing – review & editing (equal).

DATA AVAILABILITY

The data that support the findings of this study are available within the article.

NOMENCLATURE

- D Molecular diffusivity
- $d\overline{U}/dy$ The derivative of the mean velocity in the Eulerian framework
 - G Constant for determining the channel wall velocity in place Couette flow
 - H Helicity density $\mathbf{H} = \mathbf{u} \cdot \boldsymbol{\omega}$
 - H Total helicity
 - H' Helicity density for the fluctuating velocity, $\mathbf{H}' = \mathbf{u}' \cdot \mathbf{\omega}'$
 - h Half channel height
 - h' Relative helicity density
 - PDF Probability Density Function
 - Re The Reynolds number
 - R^L The Lagrangian correlation coefficient
 - Sc The Schmidt number
 - S_{ii} The local rate of strain tensor
 - TKE Turbulent kinetic energy
 - t Time
 - U The Eulerian velocity vector of the fluid at the location of the marker at time t
 - $U_{\rm c}$ The mean centerline velocity of the channel

- U_w The streamwise velocity at the wall
- \overline{U} The mean velocity
- u Velocity vector
- u' The fluctuating velocity vector
- *u** The friction velocity
- $\overline{u^2}$ The mean square of the *x*-component of the velocity of the fluid particles
- u', v', w' Fluctuating velocity components in x, y, and z directions, respectively.
 - V The Lagrangian velocity
 - x, y, z The streamwise, normal, and spanwise directions, respectively
 - X Position vector of a marker
 - X_f The displacement of a fluid particle relative to its source
 - X_o The location that a marker was released at time t_0
 - Y₀ Distance from the bottom wall of the channel for particle release at time t₀ as viscous length scale
 - \overline{Y} Average normal position of the markers

Greek symbols

- α The molecular thermal diffusivity
- Δ Change in quantity
- ϵ The turbulent dissipation rate along the trajectories of each marker
- heta' The angle between the fluctuating velocity and vorticity vectors
- ν The fluid kinematic viscosity
- π Trigonometric pi
- σ The standard deviation of the normal distribution that characterizes the random walk on the particle motion at the end of every convection step in viscous wall units
- au_{Ly} Lagrangian timescale for dispersion in the direction normal to the channel walls
- τ_w The wall shear stress
- **ω** Vorticity vector
- ω' The vorticity vector for the fluctuating velocity

Superscripts and subscripts

- () Ensemble average
- ()₀ Value of a quantity at initial time of interest
- () w Value at the wall of the channel
- ()_c Value at the center channel
- Absolute value.

REFERENCES

- ¹Z. Yan, X. Li, C. Yu, J. Wang, and S. Chen, "Dual channels of helicity cascade in turbulent flows," J. Fluid Mech. **894**, R2 (2020).
- ²H. K. Moffatt, "Helicity and singular structures in fluid dynamics," Proc. Natl. Acad. Sci. U. S. A. 111, 3663 (2014).
- ³C. Yu, R. Hu, Z. Yan, and X. Li, "Helicity distributions and transfer in turbulent channel flows with streamwise rotation," J. Fluid Mech. 940, A18 (2022).
- ⁴G. Sahoo, F. Bonaccorso, and L. Biferale, "Role of helicity for large- and small-scale turbulent fluctuations," Phys. Rev. E **92**, 051002 (2015).
- ⁵Q. Nguyen and D. V. Papavassiliou, "Using helicity to investigate scalar transport in wall turbulence," Phys. Rev. Fluids 5, 062601 (2020).

- ⁶M. M. Rogers and P. Moin, "Helicity fluctuations in incompressible turbulent flows," Phys. Fluids **30**, 2662 (1987).
- ⁷P. Nevir and R. Blender, "A Nambu representation of incompressible hydrodynamics using helicity and enstrophy," J. Phys. A: Math. Gen. **26**, L1189 (1993).
- ⁸R. B. Pelz, L. Shtilman, and A. Tsinober, "The helical nature of unforced turbulent flows," Phys. Fluids **29**, 3506–3508 (1986).
- ⁹H. K. Moffatt, "Helicity–invariant even in a viscous fluid," Science 357, 448 (2017).
- 10 H. K. Moffatt, "Transport effects associated with turbulence with particular attention to the influence of helicity," Rep. Prog. Phys. 46, 621 (1983).
- ¹¹C. G. Speziale, "On helicity fluctuations and the energy cascade in turbulence," in *Recent Advances in Engineering Science*, Lecture Notes in Engineering Vol. 39 (Springer, Berlin, Heidelberg, 1987).
- ¹²L. Biferale, S. Musacchio, and F. Toschi, "Split energy-helicity cascades in three-dimensional homogeneous and isotropic turbulence," J. Fluid Mech. **730**, 309 (2013)
- ¹³A. Campagne, B. Gallet, F. Moisy, and P. P. Cortet, "Disentangling inertial waves from eddy turbulence in a forced rotating-turbulence experiment," Phys. Rev. E 91, 043016 (2015).
- ¹⁴P. A. Davidson, Turbulence in Rotating, Stratified and Electrically Conducting Fluids (Cambridge University Press, 2013).
- $^{15}\mathrm{M.~J.~Lighthill},$ Waves in Fluids (Cambridge University Press, 2001).
- ¹⁶V. V. Gvaramadze, G. A. Khomenko, and A. V. Tur, "Large-scale vortices in helical turbulence of incompressible fluid," Geophys. Astrophys. Fluid Dyn. 46, 53 (1989).
- ¹⁷N. Yokoi and A. Yoshizawa, "Statistical analysis of the effects of helicity in inhomogeneous turbulence," Phys. Fluids A 5, 464 (1993).
- ¹⁸O. G. Chkhetiani and E. Golbraikh, "Turbulent field helicity fluctuations and mean helicity appearance," Int. J. Non-Linear Mech. 47, 113 (2012).
- ¹⁹N. Yokoi and A. Brandenburg, "Large-scale flow generation by inhomogeneous helicity," Phys. Rev. E **93**, 033125 (2016).
- ²⁰C. Srinivasan and D. V. Papavassiliou, "Direction of scalar transport in turbulent channel flow," Phys. Fluids 23, 115105 (2011).
- ²¹M. W. Scheeler, "Complete measurement of helicity and its dynamics in vortex tubes," Science 357, 487 (2017).
- ²²T. Teitelbaum and P. D. Mininni, "Effect of helicity and rotation on the free decay of turbulent flows," Phys. Rev. Lett. 103, 014501 (2009).
- ²³K. Inagaki, N. Yokoi, and F. Hamba, "Mechanism of mean flow generation in rotating turbulence through inhomogeneous helicity," Phys. Rev. Fluids 2, 114605 (2017).
- ²⁴B. Qu, A. Naso, and W. J. T. Bos, "Cascades of energy and helicity in axisymmetric turbulence," Phys. Rev. Fluids 3, 014607 (2018).
- ²⁵A. Povitsky, "Three-dimensional flow with elevated helicity in driven cavity by parallel walls moving in perpendicular directions," Phys. Fluids 29, 083601 (2017).
- ²⁶G. Wang, F. Yang, K. Wu, Y. Ma, C. Peng, T. Liu, and L.-P. Wang, "Estimation of the dissipation rate of turbulent kinetic energy: A review," Chem. Eng. Sci. 229, 116133 (2021).
- 27Y. Choi, B. G. Kim, and C. Lee, "Alignment of velocity and vorticity and the intermittent distribution of helicity in isotropic turbulence," Phys. Rev. E 80, 017301 (2009).
- ²⁸Q. Chen, S. Chen, and G. L. Eyink, "The joint cascade of energy and helicity in three-dimensional turbulence," Phys. Fluids 15, 361 (2003).
- ²⁹Y. Li, C. Meneveau, S. Chen, and G. L. Eyink, "Subgrid-scale modeling of helicity and energy dissipation in helical turbulence," Phys. Rev. E 74, 026310 (2006).
- 30 J. C. André and M. Lesieur, "Influence of helicity on the evolution of isotropic turbulence at high Reynolds number," J. Fluid Mech. 81, 187 (1977).
- ³¹A. Alexakis, "Helically decomposed turbulence," J. Fluid Mech. 812, 752 (2017).
- ³²H. K. Moffatt, "Magnetostatic equilibria and analogous Euler flows of arbitrarily complex topology. Part 1. Fundamentals," J. Fluid Mech. 159, 359 (1985).
- 33J. M. Wallace, J. L. Balint, and L. Ong, "An experimental study of helicity density in turbulent flows," Phys. Fluids A 4, 2013 (1992).
- 34P. Orlandi, "Helicity fluctuations and turbulent energy production in rotating and non-rotating pipes," Phys. Fluids 9, 2045 (1997).

- 35Q. Nguyen and D. V. Papavassiliou, "A statistical model to predict streamwise turbulent dispersion from the wall at small times," Phys. Fluids 28, 125103 (2016).
- ³⁶Q. Nguyen and D. V. Papavassiliou, "Scalar mixing in anisotropic turbulent flow," AIChE J. 64, 2803 (2018).
- ³⁷P. M. Le and D. V. Papavassiliou, "Turbulent dispersion from elevated line sources in channel and Couette flow," AIChE J. 51, 2402 (2005).
- ³⁸J. I. Polanco, I. Vinkovic, N. Stelzenmuller, N. Mordant, and M. Bourgoin, "Relative dispersion of particle pairs in turbulent channel flow," Int. J. Heat Fluid Flow 71, 231 (2018).
- ³⁹F. Hosseiniebalam, S. Hassanzadeh, and O. Ghaffarpasand, "Dispersion and deposition mechanisms of particles suspended in a turbulent plane Couette flow," Appl. Math. Modell. 37, 2417 (2013).
- ⁴⁰B. M. Mitrovic and D. V. Papavassiliou, "Effects of a first-order chemical reaction on turbulent mass transfer," Int. J. Heat Mass Transfer 47, 43 (2004).
- ⁴¹K. T. Nguyen and D. V. Papavassiliou, "Effects of a reacting channel wall on turbulent mass transfer," Int. J. Heat Mass Transfer 51, 2940 (2008).
- ⁴²P. M. Le and D. V. Papavassiliou, "A physical picture of the mechanism of turbulent heat transfer from the wall," Int. J. Heat Mass Transfer 52, 4873 (2009).
- ⁴³P. M. Le and D. V. Papavassiliou, "On the scaling of heat transfer using thermal flux gradients for fully developed turbulent channel and Couette flows," Int. Commun. Heat Mass Transfer 35, 404 (2008).
- ⁴⁴Q. Nguyen, S. Feher, and D. Papavassiliou, "Lagrangian modeling of turbulent dispersion from instantaneous point sources at the center of a turbulent flow channel," Fluids 2, 46 (2017).
- ⁴⁵D. V. Papavassiliou, "Scalar dispersion from an instantaneous line source at the wall of a turbulent channel for medium and high Prandtl number fluids," Int. J. Heat Fluid Flow 23, 161 (2002).
- ⁴⁶C. Srinivasan and D. V. Papavassiliou, "Prediction of the turbulent Prandtl number in wall flows with Lagrangian simulations," Ind. Eng. Chem. Res. 50, 8881 (2011).
- ⁴⁷ M. Lee and R. D. Moser, "Extreme-scale motions in turbulent plane Couette flows," J. Fluid Mech. 842, 128 (2018).
- ⁴⁸T. M. Schneider, F. De Lillo, J. Buehrle, B. Eckhardt, T. Dornemann, K. Dornemann, and B. Freisleben, "Transient turbulence in plane Couette flow," Phys. Rev. E 81, 015301 (2010).
- ⁴⁹D. V. Papavassiliou and T. J. Hanratty, "Interpretation of large-scale structures observed in a turbulent plane Couette flow," Int. J. Heat Fluid Flow 18, 55 (1997)
- ⁵⁰W. M. W. Gretler, "Calculation of plane turbulent Couette-Poiseuille flows with a modified k-e model," Fluid Dyn. Res. 21, 263 (1997).
- 51T. Tsukahara, H. Kawamura, and K. Shingai, "DNS of turbulent Couette flow with emphasis on the large-scale structure in the core region," J. Turbul. 7, N19 (2006).
- 52T. Dokoza and M. Oberlack, "Reynolds number induced growth of the large-scale rolls in plane Couette flow using resolvent analysis," J. Fluid Mech. 968, A23 (2023).
- 53S. Pirozzoli, M. Bernardini, and P. Orlandi, "Turbulence statistics in Couette flow at high Reynolds number," J. Fluid Mech. 758, 327 (2014).

- ⁵⁴J. Komminaho, A. Lundbladh, and A. V. Johansson, "Very large structures in plane turbulent Couette flow," J. Fluid Mech. 320, 259 (1996).
- 55R. Kristoffersen, K. H. Bech, and H. I. Andersson, "Numerical study of turbulent plane Couette flow at low Reynolds number," Appl. Sci. Res. 51, 337 (1993).
- ⁵⁶V. Avsarkisov, S. Hoyas, M. Oberlack, and J. P. García-Galache, "Turbulent plane Couette flow at moderately high Reynolds number," J. Fluid Mech. 751, R1 (2014).
- ⁵⁷S. L. Lyons, T. J. Hanratty, and J. B. McLaughlin, "Large-scale computer simulation of fully developed turbulent channel flow with heat transfer," Int. J. Numer. Methods Fluids 13, 999 (1991).
- ⁵⁸S. A. Orszag, "On the elimination of aliasing in finite-difference schemes by filtering high-wavenumber components," J. Atmos. Sci. 28, 1074 (1971).
- 59A. Günther, D. Papavassiliou, and M. Warholic, "Turbulent flow in a channel at a low Reynolds number," Exp. Fluids 25, 503 (1998).
- ⁶⁰O. L. Pham, S. E. Feher, Q. T. Nguyen, and D. V. Papavassiliou, "Distribution and history of extensional stresses on vWF surrogate molecules in turbulent flow," Sci. Rep. 12, 171 (2022).
- ⁶¹P. M. Le and D. V. Papavassiliou, "Turbulent heat transfer in plane Couette flow," J. Heat Transfer 128, 53 (2006).
- ⁶²D. Gottlieb and S. A. Orszag, Numerical Analysis of Spectral Methods Theory and Applications (Society of Industrial Applied Mathematics Monograph, Philadelphia, 1977), Vol. 26.
- ⁶³D. V. Papavassiliou, "Turbulent transport from continuous sources at the wall of a channel," Int. J. Heat Mass Transfer 45, 3571 (2002).
- ⁶⁴K. Kontomaris, "Point source dispersion in a direct numerical simulation of turbulent channel flow," Ph.D. dissertation (University of Illinois, 1991).
- 65T. J. H. K. Kontomaris, "Effect of molecular diffusivity on point source diffusion in the center of a numerically simulated turbulent channel flow," Int. J. Heat Mass Transfer. 37, 1817 (1994).
- ⁶⁶S. S. Ponoth and J. B. McLaughlin, "Numerical simulation of mass transfer for bubbles in water," Chem. Eng. Sci. 55, 1237 (2000).
- ⁶⁷C. Srinivasan and D. V. Papavassiliou, "Comparison of backwards and forwards scalar relative dispersion in turbulent shear flow," Int. J. Heat Mass Transfer 55, 5650 (2012).
- ⁶⁸S. C. Chapra, Applied Numerical Methods with MATLAB® for Engineers and Scientists (McGraw-Hill Education, 2011).
- ⁶⁹R. B. Pelz, "Velocity-vorticity patterns in turbulent flow," Phys. Rev. Lett. 54, 2505 (1985).
- 70Y. Choi, Y. Park, and C. Lee, "Helicity and geometric nature of particle trajectories in homogeneous isotropic turbulence," Int. J. Heat Fluid Flow 31, 482 (2010)
- ⁷¹N. T. K. H. Bech, N. Tillmark, P. H. Alfredsson, and H. I. Andersson, "An investigation of turbulent plane Couette flow at low Reynolds numbers," I. Fluid Mech. 286, 291 (1995).
- ⁷²B. Debusschere and C. J. Rutland, "Turbulent scalar transport mechanisms in plane channel and Couette flows," Int. J. Heat Mass Transfer 47, 1771 (2004).